Journal of Materials Chemistry B

ROYAL SOCIETY OF CHEMISTRY

PAPER

View Article Online
View Journal

Cite this: DOI: 10.1039/d5tb00737b

A comprehensive protocol for hydrogel-based bioink design: balancing printability, stability, and biocompatibility

Rency Geevarghese, [a] Joanna Żur-Pińska,[a] Daniele Parisi *[b] and Małgorzata Katarzyna Włodarczyk-Biegun *[ac]

Bioink design is one of the most challenging and time-consuming tasks in 3D bioprinting. This study provides a comprehensive framework balancing key factors such as printability (evaluated through rheological analysis), scaffold mechanical stability, and biocompatibility for developing inks based on alginate (Alg), carboxymethyl cellulose (CMC), and gelatin methacrylate (GelMA). A detailed protocol is presented, outlining the sequence of rheological tests, selecting appropriate parameters, and correlating them with printability indices (*e.g.*, fiber diameter and printability value) as well as printing conditions (*e.g.*, temperature, cross-linking time, and degree). Optimal formulations were identified as 4% Alg, 10% CMC, and GelMA at 8%, 12%, and 16% concentrations (4% Alg–10% CMC–**GelMA**). Rheological and printability functions were quantified, establishing them as benchmarks for bioink design. The thermo-responsive properties of GelMA allowed precise control of printability by modulating temperature and GelMA content. A mathematical model was employed to correlate the shear-thinning behavior, measured *via* shear rheology, and printing conditions. These bioinks demonstrated long-term mechanical stability (up to 21 days), superior mechanical performance, and enhanced cell proliferation at 4% Alg–10% CMC–16% GelMA. The dual curing approach (UV curing and $CaCl_2$ cross-linking) resulted in scaffolds with variable stiffness, showcasing their potential for gradient tissue regeneration. Notably, the protocol is adaptable to other materials and concentrations, streamlining bioink development for diverse applications in gradient tissue engineering.

Received 30th March 2025,
Accepted 5th September 2025

DOI: 10.1039/d5tb00737b

rsc.li/materials-b

1. Introduction

3D bioprinting (3DBP) has been in the limelight of the tissue engineering (TE) scientific community over the past two decades due to its potential to build complex functional tissue equivalents.[1] The technology enables obtaining 3D structures by depositing materials with embedded cells in a layer-by-layer fashion with high precision, scalability, and cost-effectiveness.[2,3] Such structures find vast applications ranging from proof-of-concept new material prints to hierarchical artificial tissues and models for drug testing and implants for regenerative medicine.[4] Various bioprinting modalities have been developed, primarily extrusion-based, jetting-based, and vat photopolymerization-based techniques, each presenting distinct advantages and limitations with respect to printability, resolution, and bioink compatibility. Extrusion-based bioprinting, the most widely adopted technique in tissue engineering laboratories, is particularly well-suited for printing highly viscous, cell-laden hydrogel systems, offering excellent flexibility in material formulation and scalability.[5,6] In contrast, jetting-based bioprinting is constrained by the requirement for low viscosity and the potential for nozzle clogging.[7] Finally, vat photopolymerization techniques are limited to photocrosslinkable materials and may pose phototoxic risks to embedded cells.[8] Given the widespread use of extrusion-based bioprinting, its high applicability in tissue engineering, the availability of suitable equipment in many laboratories, and the variety of compatible hydrogel-based materials, this paper focuses on proposing strategies for designing bioinks specifically for extrusion-based bioprinting.

Bioinks are printable formulations comprising polymeric components, cells, suitable cross-linkers, and biochemical cues.[9] Natural hydrogel-based materials (*e.g.*, alginate, cellulose, collagen, hyaluronic acid, and gelatine) with high water content, good water retention capacity, and degradability, providing a

[a] *Biotechnology Center, Silesian University of Technology, B. Krzywoustego 8, 44-100 Gliwice, Poland. E-mail: rgeevarghese@polsl.pl, joanna.zur-pinska@polsl.pl, malgorzata.wlodarczyk-biegun@polsl.pl*
[b] *Dep. Chemical Engineering, Product Technology Group, University of Groningen, Nijenborgh 3, 9747 AG Groningen, The Netherlands. E-mail: d.parisi@rug.nl*
[c] *Zernike Institute for Advanced Materials, University of Groningen, Nijenborgh 3, 9747 AG Groningen, The Netherlands. E-mail: m.k.wlodarczyk@rug.nl*

cell-friendly environment are extensively used in 3DBP.[10] Synthetic polymer-based inks such as polyethylene glycol (PEG) and polyvinyl alcohol (PVA) have also been employed in 3D printing, benefiting from their straightforward tunability to comply with tissue-specific degradation and mechanical properties. Irrespective of the hydrogel origin, designing a functional bioink demands adjustment of three primary parameters: (1) printability, (2) degradability/stability, and (3) biocompatibility. Those parameters are the prerequisites for successful bioprinting and can be controlled by the material design (composition, polymer architecture), yet very often not independently.[11]

Printability is defined as the ability of the ink to form a reproducible, sustainable 3D structure as a result of the printing process.[12] Printable material must be extrudable, flow under applied pressure, and maintain a stable and self-supporting structure after deposition on the printing stage. Printability also determines the overall structure and mechanical properties of the scaffold, which can influence the morphology, growth, and differentiation of incorporated cells and the ability of fabricated 3D structures to resemble anatomical designs.[13,14] Printability can be evaluated using the dimensionless ratios of different parameters of interest (*e.g.*, printability value Pr) and dispensing velocity ratio or dimensionless numbers (such as capillary number and Reynolds number).[15–17]

Several studies have indicated that hydrogel rheology can be a roadmap correlating printability with material properties.[18] Shear thinning, visco-elasticity, thixotropy, and yield stress were shown as essential parameters influencing the printability of a bioink.[19] Shear thinning is a non-Newtonian behavior of a fluid that decreases its viscosity with increasing shear rate, facilitating extrudability and cell survival during printing.[20] This property can be evaluated with a flow sweep test performed in a rotational rheometer. Visco-elasticity can be defined as a simultaneous existence of elastic and viscous properties described by two rheological functions – storage modulus G' (a measure of the elastic property of material's response to a small oscillatory strain) and loss modulus G'' (a measure of the viscous property of material's response to a small oscillatory strain) While viscous behavior facilitates extrusion and material flow, the dominance of elastic properties supports shape persistence after printing. The parameters G' and G'' can be derived using oscillation tests like frequency sweep, amplitude sweep, and temperature ramp.[21] A frequency sweep is performed to study the frequency-dependent behavior of the material in a non-destructive range of deformation (linear visco-elasticity). For visco-elastic liquids, the test provides information about the material's structural relaxation time (inverse frequency and the moduli crossover point (CF).[22] The shear strain amplitude sweep test is performed at a fixed frequency, typically 100 rad s^{-1}, up to a nonlinear visco-elastic regime, where the shear stress does not depend linearly anymore on the shear strain.[23] This test aids in identifying the maximum shear strain below which the linear visco-elastic regime (LVE) is ensured at a given frequency. Such a test can also provide information on the frequency-dependent yield stress (YS), describing a transition point from elastic to viscous behavior.[24] The yield stress values can be directly correlated to the concentration of polymers and extrusion pressure; the inks with high polymer content exhibit high yield stress, reflected in the elevated extrusion pressure. Thixotropy is the ability of the material to decrease viscosity at a constant shear rate. The thixotropy test mimics the actual printing conditions (before, during, and after printing) and reveals the ink's post-shear thinning structural recovery or self-healing nature.[25,26] In this test, the ink is reversibly subjected to low and high oscillatory shear deformation, and the moduli (G' and G'') are recorded. The response of ink to various stimuli (*e.g.*, temperature changes and cross-linking conditions such as UV or cross-linker addition) can also provide information about the optimal printing and cross-linking conditions.[27] The information derived from the temperature ramp test can give an insight into the G' and G'' values of inks and shear exerted on the cell embedded in the gel during printing.[28] The final stiffness of the bioprinted construct can be studied using an oscillatory time sweep test wherein G' and G'' values are measured post-curing.[29] That data is crucial in identifying the structural and mechanical resemblance of the 3D-printed scaffold to the physiological counterparts. Numerous attempts have been made to link rheology and printability.[30,31] However, a well-defined experimental protocol to correlate shear rheology and 3D-printing printing for ink design is missing.

The scaffold post-printing stability or degradability in the appropriate culture media is defined as the ability of the printed structure to maintain its integrity, shape, and functionality over time.[32] This stability is crucial to ensure that the scaffold supports biological processes such as cell growth, tissue development, or drug delivery, and it does not degrade prematurely or lose its structural properties.[33,34] This property primarily depends on the components' interaction, cross-linker types, and their density.[35] For instance, alginate (Alg), widely cross-linked using $CaCl_2$, forms a physical temporary (ionic interactions) network that, in cell media conditions, slowly releases calcium and, consequently, alginate chains. In contrast, photo cross-linking using methacrylate (MA) systems like gelatin methacrylate (GelMA) or hyaluronic acid methacrylate forms a covalent bond in the presence of photoinitiators, providing long-term stability to the system in physiological media. Further, the type and cross-linking degree define the swelling property of the material. Properly tuned stability will ensure initial support for cell attachment, favoring cell survival and controlled degradation, allowing eventual replacement of the scaffold with the cell-produced extracellular matrix.[36]

In addition to ensuring the scaffold's printability and post-printability stability, biocompatibility plays a crucial role by promoting proper cell attachment, maintaining high cell viability, and supporting tissue-specific differentiation, making it essential for regenerating diverse tissues.[37] The chemical and biological composition of a bioink and the printed scaffold's topology, stiffness, and stability are determinant factors for cell survivability and tissue regeneration.[38] The availability of cell attachment domains can help with initial adherence. For instance, gelatin has been identified as a promising bioink

component endorsing cell growth due to the presence of cell attachment peptide motifs like RGD (arginine–glycine–aspartic acid).[39] Additionally, the cross-linking approaches used to tune the printability and stability of the scaffolds and the degradation of the scaffold products need to be non-toxic for the growth and proliferation of encapsulated cells.[40] This shows that printability, stability, and biocompatibility are not independent and must be adjusted carefully to counterbalance each other.

Recent advancements in hydrogel-based bioinks have focused on optimizing key material properties such as printability, structural stability, and biocompatibility—especially in systems based on alginate, gelatin, GelMA, and emerging materials like SilkMA (a methacrylated silk fibroin derivative). These materials exhibit broad tunability: GelMA hydrogels can achieve storage moduli (G') ranging from $\sim$3 kPa up to $>$100 kPa depending on polymer concentration and UV exposure conditions, while alginate hydrogels range from 1–50 kPa depending on calcium content. The optimal printability for cell-laden alginate, assuring high cell viability, is typically associated with G' values below $\sim$10 kPa.[41–44] Study have linked lower GelMA concentrations—and consequently lower stiffness—to enhanced cell viability, particularly in neuronal and myogenic applications.[45] However, precise G' thresholds ensuring safe printing conditions are not consistently defined in the literature, emphasizing the need for standardized rheological benchmarks in bioink design. SilkMA based bioprinting can reach up to $\sim$640–770 Pa or more, ensuring biocompatibility.[45] Balancing shear modulus is critical, as overly stiff inks increase extrusion forces, potentially compromising cell viability. Many existing studies focus on either mechanical optimization or biological compatibility separately.[46] What is often missing is an integrated framework that quantifies rheological behavior, print fidelity, stability in culture, and cytocompatibility in a unified workflow. Therefore, this work provides general guidance and tips on bioink design by balancing three factors: printability (assessed by rheology and printability quality indices), post-printability stability (assessed from weights of the printed construct placed in media), and biocompatibility (assessed by live–dead and Alamar blue assay).

The bioink based on gelatin and alginate was chosen for the study due to its broad applicability in 3D bioprinting.[47] Specifically, the ink comprising Alg, CMC, and GelMA was prepared in phosphate-buffered saline (PBS). Alg and CMC (an anionic cellulose-derived emulsifier) were chosen primarily to tune the formulation's printability. Previous studies have shown that Alg/CMC inks possess an electrostatic interaction, forming a full-interpenetrating polymeric network resulting in improved mechanical properties, swelling capacity, and biodegradability.[48,49] Alg and GelMA were intended to enhance the stability of the 3D construct *via* ionic cross-linking (by Alg–Ca interactions) and photo cross-linking (using UV curing of gelatin methacrylate groups in the presence of photo-initiator), respectively.[50] The addition of GelMA was also meant to improve biocompatibility. The inks with good printability, stability, and biocompatibility were identified. A correlation between rheological properties and printed structure was established, the apparent shear rate was estimated using a mathematical model, and apparent shear viscosity and shear stress were quantified. Post-printing-cross-linked scaffolds were subjected to stability and cell culture tests. Overall, this study provides an easy-to-apply, systematic, and reproducible toolset for developing well-printable bioinks without compromising stability or biocompatibility.

2. Materials and methods

2.1. Chemicals

Alginic acid sodium salt from brown algae (high viscosity), sodium carboxymethyl-cellulose (medium viscosity), gelatin from porcine skin (gel strength 300, Type A), methacrylate anhydride, lithium phenyl-2,4,6-trimethylbenzoylphosphinate (LAP), fluorescent diacetate (FDA), snakeskin dialysis tubing (10k MWCO), Dulbecco's Modified Eagle's Medium (DMEM)-high glucose media, trypsin–ethylenediamine tetraacetic acid solution and pencillin–streptomycin (Pen–Strep) were purchased from Sigma Aldrich. Other reagents were purchased from the respective companies: fetal bovine serum (Eurax), heat-stable recombinant human beta fibroblast growth factor (β-FGF) (Gibco), propidium iodide (PI) (Acros organics), $CaCl_2$ anhydrous (Chemat), Alamar blue (Bio-rad) and 1$\times$ PBS (VWR). All the samples were used as purchased, with no further purification or treatment.

2.2. Ink preparations

Alg–CMC inks at different concentrations (w/v) were used for the study (first and second bolded columns in Table 1). 25% Alg stocks (w/v) were prepared in PBS by overnight stirring at 200 rpm. PBS was chosen as a solvent to maintain the pH of

Table 1 Composition of different studied material mixtures[a]

CMC group		Alg group		GelMA group
4% Alg–**CMC**	6% Alg–**CMC**	4% CMC–**Alg**	6% CMC–**Alg**	4% Alg–10% CMC–**GelMA**
4% Alg–6% CMC	6% Alg–6% CMC	4% CMC–6% Alg		4% Alg–10% CMC
4% Alg–8% CMC	6% Alg–8% CMC	4% CMC–8% Alg	6% CMC–8% Alg	4% Alg–10% CMC–8% GelMA
4% Alg–10% CMC	6% Alg–10% CMC	4% CMC–10% Alg	6% CMC–10% Alg	4% Alg–10% CMC–12% GelMA
4% Alg–15% CMC	6% Alg–15% CMC	4% CMC–15% Alg	6% CMC–15% Alg	4% Alg–10% CMC–16% GelMA

[a] The table summarizes different mass concentrations (w/v) of Alg, CMC, and GelMA-containing inks studied. The components highlighted in bold imply that the concentration of this particular component was varied in respective combinations, and the exact representation is used throughout the manuscript. For instance, 4% Alg–**CMC** indicates 4% Alg–different concentrations of CMC.

the ink in physiological conditions. The CMC groups were prepared by uniformly mixing powdered CMC (different concentrations) with 4% and 6% Alg solution (from 25% Alg) to obtain 4% Alg–**CMC** and 6% Alg–**CMC**, respectively (first column in Table 1; the component highlighted in bold implies that its concentrations were varied in the respective mixtures). Similarly, Alg groups were obtained by mixing powdered (4% and 6%) CMC with different concentrations of Alg (from 25% Alg) to obtain 4% CMC–**Alg** and 6% CMC–**Alg**, respectively (second column in Table 1). For both CMC and Alg groups, the components were mixed thoroughly using a sterile spatula, followed by overnight shaking of the samples at 37 °C to allow the homogenous mixing of the elements. All formulations were prepared in triplicate batches under controlled temperature (37 °C) and identical mixing protocols to ensure reproducibility. The Alg and CMC concentrations below 4% were not chosen for the study as in the preliminary studies the viscosity curve of pure 2% Alg and 2% CMC depicted a low shear viscosity value in the range of 1 Pa s. Which is likely to give collapsing strands post-printing (Fig. S7).[51]

4% Alg–10% CMC–**GelMA** inks (third bold column in Table 1) were prepared as follows. 8% Alg and 40% GelMA stocks (w/v) were prepared separately in PBS by stirring the solutions at 100 rpm overnight at 37 °C. Next, 4% Alg (from 8% Alg) was mixed with GelMA (from 40% GelMA) at 37 °C using a sterile spatula to obtain 4% Alg–GelMA. Finally, the powdered 10% CMC was combined with a 4% Alg–GelMA solution to obtain 4% Alg–10% CMC–**GelMA**. The mixture was kept overnight in a shaker at 37 °C. On a subsequent day before printing, the 0.25% LAP photoinitiator was added (from 5% LAP stock prepared in PBS) and mixed homogeneously using a sterile spatula while maintaining ink in a water bath at 37 °C. Before loading in the printing cartridge, the inks were centrifuged at 1000 rpm for 15 min at 37 °C to eliminate air bubbles. The importance of maintaining the component mixing sequence and temperature control during bioink preparation was validated through a series of experiments (as shown in Fig. S15 and S16). All bioink formulations were prepared in triplicate under controlled temperature (37 °C) and identical mixing protocols to ensure reproducibility.

2.3. Printing of different inks

The quality of different inks was studied by printing two-layered square scaffolds of 10 × 10 mm dimension with 1.5 mm 2 layer distance and 7.5 mm s^{-1} printing speed. The scaffolds were printed using a GeSiM 3D bioscaffolder. The minimum pressure needed to extrude inks was used, which significantly depends on the polymer concentration and is reported later in the text for each sample. Four-layered square constructs were printed at the optimized extrusion pressure, defined as the minimum required for stable filament formation. As this parameter remained constant across replicates, it is reported as a single representative value per formulation. 30% relative humidity was recorded in the hood during printing. Alg–CMC combinations (detailed in Table S1) were printed using a plastic conical nozzle of 250 μm orifice diameter. 4% Alg–10% CMC–**GelMA** scaffolds were printed using a metallic nozzle of 200 μm orifice diameter to maintain the temperature of 37 °C. Plastic nozzles could be employed in the case of Alg–CMC combinations due to the component's non-thermoresponsive properties. 4% Alg–10% CMC–**GelMA** was maintained in a water bath at 37 °C, and before printing, it was pre-heated to 37 °C in the printing cartridges for 10 min. The temperature of the printing cartridge was set at 37 °C. These precautions were taken to ensure good extrudability and ease cell survival when cells were mixed with 4% Alg–10% CMC–**GelMA** for printing.

Following printing, 3D scaffolds generated using 4% Alg–**CMC** and 4% CMC–**Alg** were cross-linked with 0.1 M $CaCl_2$ for 4 min. Scaffolds printed with 4% Alg–10% CMC–**GelMA** were dually cross-linked—firstly using a UV pen (of GeSiM 3D bioscaffolder) at 25 mW cm^{-2} for 60 s (at the height of 25 mm from the printing stage), secondly by 0.1 M $CaCl_2$ treatment for 4 min.

The images of printed scaffolds were immediately captured using a stereomicroscope (SZ-PT Olympus) to study printability quality indices. Printability assessments were performed in duplicates from triplicate batches under fixed printing parameters, and printability metrics were recorded for each batch until a continuous, smooth-stranded square mesh was consistently achieved. The printability quality indices – FD, defined by the printed scaffold's fiber diameter, were measured using ImageJ software from the images and were compared to the nozzle size. The diameter of the six vertical strands from the center of the scaffolds was measured in triplicates, and its closeness to nozzle size was studied. To define well-printable ink, the calculated FD needs to be in the range of the used nozzle size (250 μm and 200 μm, respectively).

In other printability quality indices, ink printability value (Pr) was calculated based on eqn (1).[52]

$$\mathrm{Pr} = \pi/4 \times 1/C \quad (1)$$

where C is the printed grids' circularity (measured using ImageJ software).

Using ImageJ, the inner circumference of the 25 square pores in the center was measured, substituting printed grids' circularity (C) to eqn (1). The Pr value describes the correlation between ink printability and shape retention ability. An ink with good printability is anticipated to depict smooth, continuous extrudable fiber and retain the square pores (defined by G-code) post-printing (Pr ≈ 1). Inks with poor printability, give collapsing strands with circular pores (Pr < 1). As the total polymer content in an ink increases, wavy, irregular strands are observed (Pr > 1) (see also Fig. S3G). Studies have also proved that it is best to set the acceptable Pr value between 0.9 and 1.1 rather than one particular value, as precisely calculating this parameter is challenging. Pr values can vary depending on the region (center or sides) of the printed scaffold from where the value is estimated.[52]

The best printability was characterized by a Pr value in the range 0.9–1.1 and FD ≃ 250 μm and 200 μm for different Alg–CMC combinations and 4% Alg–10% CMC–**GelMA** inks, respectively.

2.4. Rheological tests

2.4.1. Measurements for inks containing Alg and CMC only. Samples were loaded in the rheometer (TA Discovery Hybrid 2), and a thermal equilibration at 37 °C was maintained. Reproducibility was further assessed using statistical analysis Consequently, flow sweep, shear strain amplitude sweep, and frequency sweep tests of 4% Alg–**CMC** and 4% CMC–**Alg** were performed in triplicates, using a solvent trap, to minimize water evaporation. Flow sweep tests were performed using a cone and plate geometry with a 20 mm diameter and 1° cone angle. The measuring gap was 200 μm, and the shear rate varied from 0.1 to 1000 s^{-1}. Oscillation tests were performed using a 20 mm parallel plate at a gap of 200 μm. In a shear strain amplitude sweep, the angular frequency was set to 0.1 rad s^{-1}, varying the oscillation strain from 0.1 to 1000(%), while in the frequency sweep experiments, the strain was set to 1% (within the visco-elastic regime), and the angular frequency was varied from 0.1 to 500 rad s^{-1}. The shear strain amplitude sweep test determined the yield stress value at 0.1 rad s^{-1}. The yield stress value was derived as the oscillation stress value corresponding to G' and G'' cross-over points in the amplitude sweep tests (Fig. S3H).[53] Rigorously, the yield stress is calculated at zero deformation.[54] In this study, it was estimated at the lowest frequency possible, 0.1 rad s^{-1}. Next, frequency sweep tests were performed, which helped assess the crossover frequency (CF) value, whenever detectable in the probed frequency range. The structural relaxation time defines the material's ability to relax stresses fully. Ideally, optimal inks that maintain a non-collapsing structure post-printing are expected to show a visco-elastic solid behavior ($G' \gg G''$) with cross-over at low frequencies (<0.01 rad s^{-1}) or no CF at all.[23,55,56] In contrast, inks with crossover at higher frequencies tend to flow, which may lead to collapsing of printed structures.

2.4.2. Measurements for optimized inks: 4% Alg–10% CMC and 4% Alg–10% CMC–GelMA. 4% Alg–10% CMC and 4% Alg–10% CMC–**GelMA** were subjected to flow sweep (shear rate varied between 0.001 to 1000 s^{-1}), shear strain amplitude sweep, frequency sweep, and thixotropic tests at 37 °C as described in 2.4.1. The shearing time at each shear rate was set to 800 s (based on the start-up of shear rate experiments) to ensure a steady-state viscosity value at each shear rate in a flow sweep (as shown in Fig. S8A). The amplitude sweep test was performed at both 100 rad s^{-1} and 0.1 rad s^{-1} varying the strain from 0.1 to 1000%. Amplitude sweep was first performed at 100 rad s^{-1} to identify the LVE so that LVE of all other (lower) frequencies falls in this spectrum (Fig. S9A). Further YS was determined using the amplitude sweep was performed at 0.1 rad s^{-1} to resemble the yield stress closest at zero shear rate (Fig. S9B).

The thixotropic test was performed in oscillation mode, subjecting the inks to 1% and 1000% alternative oscillation strains at an angular frequency of 0.1 rad s^{-1}. Temperature ramp was conducted at a rate of 0.1 °C min^{-1} at an oscillation strain and angular frequency of 1% and 0.1 rad s^{-1}, respectively. The G' and G'' of non-cross-linked samples and cross-linked hydrogel (UV, with $CaCl_2$, and both) were measured using a time sweep test at 0.1 rad s^{-1} angular frequency and 1% strain. The storage modulus was used as a quantity to measure stiffness. A high value of G' means that the polymer behaves more stiffly under dynamic loading. For UV curing tests, 0.25% LAP photoinitiator was added to 4% Alg–10% CMC–**GelMA**, followed by 3-step sample testing using a UV accessory of the rheometer. (1) In the UV curing test, the G' and G'' of non-cured samples were tracked for 90 s, followed by curing at 25 mW cm^{-2} for 280 s. UV curing power optimization was performed in a wide range of power (5, 25, 50, and 75 mW cm^{-2}); the measurements details are mentioned in SI (Fig. S1). (2) The storage modulus of $CaCl_2$ cross-linked inks was studied using an immersion cap. An immersion cap is an accessory used to maintain the solvent around the sample and obtain the measurements while cross-linking. The time sweep of untreated inks was first measured for 180 s, followed by 0.1 M $CaCl_2$ addition to the immersion cup, around hydrogel, and measurements for 400 s. (3) To measure the final modulus of dual cross-linked (UV cured and $CaCl_2$ cross-linked) inks. First, the modulus of non-crosslinked inks was measured, followed by UV curing of inks at 25 mW cm^{-2} for 60 s, subsequent 0.1 M $CaCl_2$ treatment for 4 min, and time sweep measurements of inks for 600 s. A temperature ramp (at a rate of 0.1 °C min^{-1}) of dually-cured inks was performed to study the thermal responsiveness of the double-crosslinked inks, at an oscillation strain and angular frequency of 1% and 0.1 rad s^{-1}, respectively (Fig. S2).

Further, the estimation of shear thinning degree and the apparent shear rate, shear viscosity and shear stress values of 4% Alg–10% CMC–**GelMA** during printing was performed as described in Section 2.5. Rheological tests were conducted in duplicate from triplicate batches, and results were reported as mean ± standard deviation.

2.5. Mathematical modeling

A mathematical model was used to calculate the apparent shear rate during printing and correlate the estimated apparent shear stress to yield stress deduced from the amplitude sweep test (described in Section 2.3). First, the experimental flow curve was fit to a power-law function (eqn (2)), where the shear thinning coefficient (a and b) and power-law index n ($n = 1 - b$) were determined.[20] In the current study, curve fitting of the plot was done using Origin software. Secondly, the power-law index n was used to calculate the apparent shear rate. To this end, eqn (3), a model widely used to evaluate the resolution of well-printable ink, was employed.[31,57] The diameter of the 3D-printed filaments was derived from Table 4, while diameter of the printing nozzle and printing speed were set to 4×10^{-4} m and 7.5×10^{-3} m s^{-1}, respectively. The selected model is the best fit for the study as it allows the determination of apparent shear using power law indices and printing parameters.

$$\text{Power law equation: } \eta = a(\gamma)^{(b)} \tag{2}$$

where, η – is the apparent viscosity (Pa s). γ – is the shear rate (s^{-1}). a and b – are shear thinning coefficients.

$$\dot{\gamma} = \left(\frac{3n+1}{4n}\right) \cdot \left(\frac{8d^2}{D^3}\right) v \tag{3}$$

where, $\dot{\gamma}$ – is the apparent shear rate (s^{-1}). n – is the power law index. d – is the diameter of printing nozzle (m). D – is the

diameter of printed strands (m) (mentioned in Table 4). v – is the printing speed (m s^{-1}).

The apparent shear viscosity was then calculated using eqn (2) by substituting the apparent shear rate and coefficients. Shear stress, defined as viscosity times the shear rate, was therefore estimated by multiplying apparent viscosity with apparent shear rate. The apparent shear stress values derived were thereafter compared with the yield stress. Apparent shear rate is typically well above the determined yield stress, meaning the shear stress experienced by ink during printing is higher than the initial force required to initiate flow in the system. The model thereby serves as an effective tool in identifying the link between the yield stress and the apparent shear stress.

2.6. Shape fidelity determination in complex 3D constructs

To evaluate the shape fidelity, resolution, and structural stability of the optimized ink (4% Alg–10% CMC–16% GelMA), a series of constructs was printed and imaged macroscopically. Constructs were printed with varying geometries, infill distances, and layer heights. The printing resolution was evaluated by designing grid structures with different infill spacings (0.25 mm, 0.5 mm, 1 mm, and 1.5 mm). Geometric fidelity was assessed by printing various shapes, including triangles, hexagons, and polygons. To test the self-supporting capability and structural integrity, multi-layered grid constructs (4-layer and 10-layer) were imaged before cross-linking. 20-Layered constructs were further imaged after UV cross-linking. Structural stability of 10-layered constructs under biological conditions was assessed by incubating the constructs in DMEM supplemented with 10% FBS and 1% Pen–Strep for up to 7 days.

2.7. Study on scaffold's post-printing stability

The 3D scaffolds were printed in triplicates on 18 mm × 18 mm square coverslip using 4% Alg–10% CMC and 4% Alg–10% CMC–**GelMA** inks. A dual-cross-linking approach was used (as described in Section 2.4) after placing the scaffolds in a sterile 3 mm Petri dish. Next, the scaffolds were washed thrice with sterile PBS to remove the $CaCl_2$ remnant left after $CaCl_2$ cross-linking and 3 mL of DMEM media supplemented with 10% FBS and 1% Pen–Strep was added, to mimic the cell culturing conditions. The scaffolds were incubated at 37 °C for 21 days. The media was changed every second day, and the weights of the samples were taken on the day of printing (D0) after removing the media with the pipette. Same procedure was followed for subsequent days (D1, D5, D7, D14, and D21), and the residual weight (%) was calculated using eqn (4):

$$\text{Residual weight (\%)} = (W_f/W_i) \times 100 \quad (4)$$

where W_f – is the final weight (mg) of inks post-incubation in media and W_i – is the initial weight (mg) of the scaffolds before incubation in media.

To qualitatively assess the structural integrity of the scaffolds under culture conditions, macroscopic images of 4-layered 3D bioprinted constructs composed of 4% Alg–10% CMC–16% GelMA with primary human fibroblasts were captured. Bioink preparation, cell density, and culturing of 3D bioprinted scaffolds in DMEM supplemented with FBS and penicillin-streptomycin (Pen–Strep) were performed as detailed in Section 2.7. Images were captured on days 1, 5, and 7 to monitor shape retention and overall stability over time.

2.8. Cell study

Primary fibroblast human cells were cultured in DMEM media supplemented with 10% FBS, 1% Pen–Strep, and 1 ng mL^{-1} β-FGF in an incubator at 5% CO_2 and 37 °C. After reaching 80% confluency, the cells were passaged using 0.25% trypsin. Cells in 3–5 passages were used. 4% Alg–10% CMC–**GelMA** inks were prepared under sterile conditions (as described in Section 2.2) and maintained in a water bath at 37 °C. The sequence of component mixing, along with maintaining temperature control at 37 °C during bioink preparation, is of paramount importance. After 0.25% LAP photo-initiator was added, 1 million cells per mL suspended in supplemented DMEM were incorporated, and the bioink was gently mixed for approximately 30 seconds at 37 °C with a sterile spatula, as demonstrated by the experimental results presented in Fig. S15 and S16. Cell-laden scaffolds were printed on sterile triplicates 18 mm × 18 mm square coverslips using a GeSiM 3D bio-scaffolder. 4 layered square designs were printed with optimised extrusion pressure (as mentioned in Table 4). 3D constructs were dually cured (as described in Section 2.4). All the scaffolds were placed in 3 mm Petri dishes, washed thrice in sterile PBS, and cells in the scaffolds were cultured in a DMEM medium supplemented with 10% FBS and 1% Pen–Strep for 7 days. Live–dead assay was performed at days 1, 5 and 7 using fluorescent diacetate (FDA) for live cell and propidium iodide (PI) for dead cell staining. FDA stock (5 mg mL^{-1}) prepared in acetone and PI stock (2 mg mL^{-1}) prepared in PBS were diluted in PBS to the final concentrations of 5 μg mL^{-1} and 5 μg mL^{-1}, respectively. The 3D bioprinted scaffolds were washed with PBS, followed by the addition of staining solution and incubation for 20 min at 37 °C. Next, the scaffolds were washed thrice with PBS with a 5-minute incubation time. Confocal imaging (Olympus Fluoview FV3000) was performed on the scaffolds at 10× magnification. The cell metabolic activity in the printed scaffolds (n = 3) at days 1, 5 and 7 was studied using Alamar blue assay according to the protocol provided by the manufacturer. Briefly, 10% bio blue solution (1.5 mL) prepared in fresh media was added to each scaffold cultured in a 3 mm Petri dish and incubated at 37 °C for 4 hours. 200 μL of reagent from each sample were transferred to black-colored 96 well plates, and fluorescence at excitation and emission wavelengths of 560 and 590 nm were studied using a spectrofluorometer (Varioskan Lux, Thermo Fischer Scientific). The same scaffolds were washed twice with PBS and cultured for subsequent days upon the addition of supplemented DMEM. The cell metabolic activity was calculated using eqn (5).

$$\text{Alamar blue reduction (\%)} = \frac{(F1 \text{ test agent} - F1 \text{ untreated control})}{(F1\ 100\% \text{ reduced Alamar blue} - F1 \text{ untreated control})} \times 100 \quad (5)$$

where, $F1$ test agent – fluorescent values at 590 nm of scaffolds with cells. $F1$ untreated control – fluorescent values at 590 nm of

scaffolds without cells. *F*1 100% reduced Alamar blue – fluorescent values at 590 nm of autoclaved 10% Alamar blue prepared in media.

The higher the value of Alamar blue reduction, the higher cell metabolic activity is anticipated.

Sterilization protocols were carefully implemented to ensure aseptic conditions during bioink preparation and cell encapsulation. 8% alginate stock solution was prepared in sterile PBS and sterilized by autoclaving at 121 °C for 20 minutes. Lyophilized GelMA and powdered CMC were sterilized by UV exposure under a laminar flow hood for 20 minutes, and a 40% GelMA stock solution was subsequently prepared in sterile PBS. The 5% photoinitiator (LAP) stock solution was also prepared in sterile PBS using beads that had been sterilized in 70% ethanol prior to use. All printing accessories—including metallic cartridges, nozzles, pressure regulators, and spatulas—were immersed in 70% ethanol overnight before use. Additionally, consumables such as Eppendorf tubes, pipette tips, and water bath containers were autoclaved and UV-sterilized before use. All bioink preparation steps were conducted under aseptic conditions within a laminar airflow hood. No visible signs of microbial contamination (*e.g.*, turbidity or fungal growth) were observed in the cell-laden scaffolds cultured for up to 7 days, confirming the effectiveness of the sterilization procedures.

2.9. Statistical analysis

All results were reported as mean values ± standard deviation from duplicate measurements across triplicate batch, and statistical differences were calculated using a two-way analysis of variance (ANOVA) and a Tukey multi-comparison *post hoc* test, performed using GraphPad Prism software. Differences with a p-value <0.001 and $^{*}p$-value <0.05 were considered significant.

3. Results and discussion

3.1. Printing and rheology of 4% Alg mixed with different CMC concentrations (4% Alg–CMC)

Inks with 4% Alg and different concentrations of CMC were printed, and printability quality indices, FD and Pr, were calculated to assess material printability. FD value was measured by correlating the diameter of printed strands with the nozzle orifice diameter of 250 μm. Adding 6% or 8% of CMC to 4% Alg was insufficient for a well-printable scaffold with inhomogeneous thick strands. In such conditions, Pr ≈ 0.8 and FD ≈ 270–260 μm upon printing with extrusion pressure of 85–135 kPa (Fig. 1A and B). As CMC concentration increased to 10%, the inks extruded at 190 kPa pressure exhibited Pr = 0.95 ± 0.08 and FD = 250 ± 20 μm, maintaining perfect square grids post-printing (Fig. 1C). As the CMC content increased to 15%, Pr = 0.96 ± 0.02 and FD = 240 ± 20 μm were obtained at 475 kPa extrusion pressure (Fig. 1D). Further increase of CMC to 20% with YS of 1473 ± 20 Pa required an extrusion pressure of 598 kPa, and the printed scaffolds presented non-smooth discontinuous strands with FD = 200 ± 25 μm. Due to the broken or non-uniform strands, the estimation of Pr value was not possible (Fig. S3G). The analysis revealed that increased CMC concentrations improved 4% Alg–CMC ink printability. The inks above a threshold concentration of CMC (10%) were well-printable up to *ca.* 15% CMC addition.

Rheological tests were performed to correlate the obtained printing results with material composition. The flow sweep

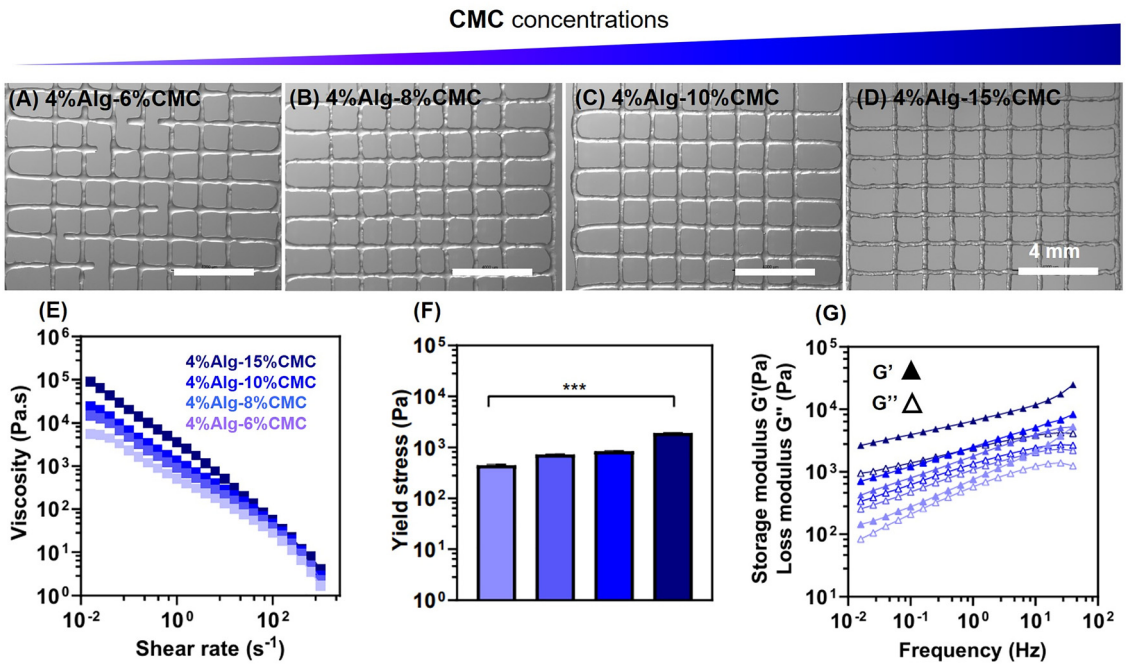

Fig. 1 Correlation between printing and rheology of 4% Alg–CMC. (A)–(D) Represents stereomicroscopic images of 3D-printed scaffolds. (E)–(G) Depict the inks' flow sweep, the yield stress obtained from shear strain amplitude sweep and frequency sweep, respectively.

tests revealed that 4% Alg inks with all tested concentrations of added CMC were characterized by decreasing viscosity with increasing shear rate, proving the shear-thinning nature of the inks (Fig. 1E). The shear strain amplitude sweep test was performed, which showed $G'' > G'$ irrespective of the applied strain for low-concentration gels (*i.e.*, 4% Alg–4% CMC, see Fig. S3H). However, as the CMC polymer concentration increased (*i.e.*, 4% Alg–6% CMC, see Fig. S3H), the gel depicted a $G' > G''$ at a lower strain, gradually showing a crossing-over of G' over G'' as the strain increased. YS derived from the test showed that the value significantly increased from 54 ± 15 Pa to 1473 ± 20 Pa as the CMC content increased from 6% CMC to 20% CMC (Fig. S3I). The frequency sweep showed solid-like behavior ($G' > G''$) at high frequencies for the 4% Alg–4% CMC ink (low CMC content) and a crossover frequency at 2.52 Hz, corresponding to a 0.39 s terminal relaxation time. This correlates with the observation that 4% Alg–4% CMC ink relaxed and collapsed relatively fast after printing and could not maintain its shape (see Fig. S3J). All inks above 4% Alg–6% CMC showed a dominance of elastic behavior ($G' > G''$) across the whole frequency range probed in the experiments (Fig. S3J). Also, the G' value showed an increase from 142 Pa to 2648 Pa as CMC concentration increased (Table 2). Thus, when the concentration of the CMC polymer increased, the YS and G' values increased, and no CF was observed.

To conclusively deduce the most suitable ink, the derived rheological parameters (YS, G', and CF) of inks and extrusion pressure were associated with the printability quality indices (FD and Pr value) (see Table 2). As CMC content increased, *i.e.*, 4% Alg–10% CMC ink depicted an optimal printability quality indices value with Pr = 0.95 ± 0.08 and FD = 250 ± 10 μm (Fig. 1C and Table 2), at relatively lower printing pressure (190 Pa), making it the suitable candidate for further studies. Low printing pressure is a desirable property for developing bioinks to decrease the probability of cell death due to the high pressure. This model system suggested that the desired rheological properties for printing are: (1) YS above 300 Pa, (2) no CF, (3) $G' > G''$ and in the range of 400–500 Pa using 4% Alg in combination with less than 20% CMC.

The rheology and printing test of 6% Alg–**CMC** was also performed to check if increasing the CMC content improves printing. The same trends were observed in rheological properties and printing as for 6% Alg–**CMC** (Fig. S4). 6% Alg–8% CMC with YS = 1901 ± 20 Pa, G' = 450 ± 2 Pa and no CF was extruded at a pressure of 200 kPa, giving prints with FD = 262 ± 15 μm and Pr = 0.9 ± 0.004, showing good printability. A higher YS required to obtain a well-printed strands from 6% Alg–**CMC** with properties comparable to 4% Alg–10% CMC, therefore printing of this material with cells could be challenging.

3.2. Printing and rheology of 4% CMC mixed with different Alg concentrations (4% CMC–Alg)

Pure (2% to 12%) Alg, pure (2% to 12%) CMC (Fig. S7A–D), and 4% Alg–CMC all show a shear thinning and visco-elastic property; therefore, how those components contribute to printability of the system had to be answered. For this reason, we also decided to investigate 4% CMC–**Alg** inks, with fixed CMC concentrations with Alg concentrations ranging from 6% to 15% Alg (Fig. 2A–D). It was observed that 4% CMC with (6% and 8%) Alg and 4% CMC with (10% and 15%) Alg depicted Pr in the range of 0.8 and 0.95, respectively (Table 3). As Alg concentration increased from 6% to 15%, FD values were close to a nozzle diameter of 250 μm, but a higher extrusion pressure varying from 70 to 370 kPa was required (Table 3). It can be concluded that Alg at lower concentrations (of 6% and 8%) did not improve printability (Fig. 2A and B); however, increasing Alg concentrations above 10% had a significantly impact (Fig. 2C and D). Further, 4% CMC–20% Alg depicted optimal printability quality indices with FD = 255 ± 20 μm and Pr = 1 ± 0.02 (Fig. S5G); however, a required printing pressure was very high (*i.e.* 590 kPa). 4% CMC–10% Alg (with total polymer content resembling 4% Alg–10% CMC) was extrudable at a pressure of 160 kPa and gave prints with Pr = 0.95 ± 0.05 and FD = 280 ± 20 μm. The FD value is higher than the nozzle size of 250 μm. This is due to the weak physical interaction between the polymeric chains of Alg and increased collapsing of the material when compared to 4% Alg–10% CMC ink.[49,58] Thus, to obtain a well-printable formulation from the 4% CMC–**Alg** group, relatively high polymer content was required, and bioprinting of the ink with high extrusion pressure would be required, which makes the system less favorable for bioink (*i.e.* for printing with enclosed cells).

The rheological testing proved the shear thinning property of 4% CMC–**Alg** inks (Fig. 2E). The amplitude sweep test showed that 4% CMC with 4% and 6% Alg demonstrated $G'' > G'$ irrespective of the strain, with no yield stress values (Fig. S5H). Increasing Alg concentration to 8% led to $G' > G''$, with a yield stress of 125 ± 10 Pa (Fig. S5H and I). The yield stress value significantly increased as Alg content increased (Fig. S5I). In the frequency sweep test, 4% CMC–4% Alg and 4% CMC–6% Alg depicted a cross-over frequency at 2.5 Hz (with relaxation time = 0.4 s) and 1.6 Hz (with relaxation time = 0.625 s) (Fig. S5K), respectively. 4% CMC with 8%,10%, and 15% Alg revealed $G' > G''$ in the range of frequencies, implying

Table 2 Summarizes the extrusion pressure, printability quality indices (FD and Pr values), and rheological parameters (YS, G' and CF). *** Represents a significant difference with a p-value < 0.001

Inks	Pressure (kPa)	YS (Pa)	CF (Hz)	G' (Pa)	FD (μm)	Pr value
4% Alg–6% CMC	85	54 ± 15	NA	142 ± 2	270 ± 30	0.83 ± 0.06
4% Alg–8% CMC	135	154 ± 10	NA	420 ± 3	260 ± 30	0.85 ± 0.02
4% Alg–10% CMC	190	308 ± 10	NA	487 ± 2	250 ± 20	0.95 ± 0.08
4% Alg–15% CMC	475	1082 ± 15	NA	2648 ± 4	240 ± 20	0.96 ± 0.02

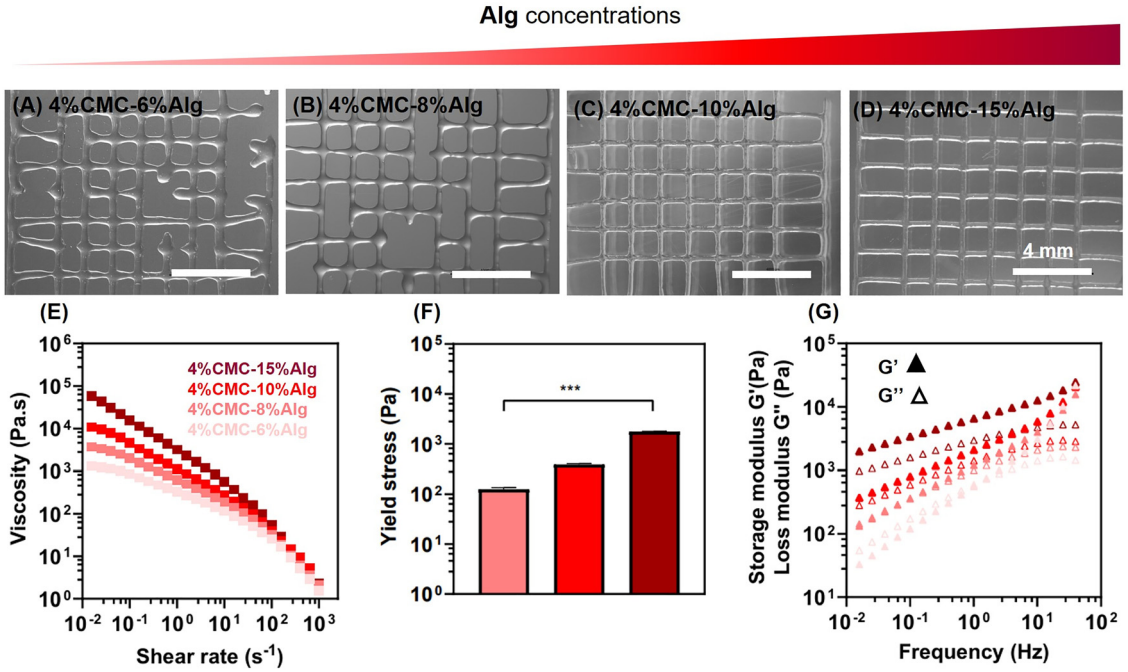

Fig. 2 Correlation between printing and rheology of 4% CMC–Alg. (A)–(D) Represent stereomicroscopic images of 3D-printed scaffolds. (E)–(G) Depict the inks' flow sweep, the yield stress deduced from amplitude sweep and frequency sweep, respectively.

Table 3 Summarizes the extrusion pressure, printability quality indices (FD and Pr value), and rheological parameters (YS, G' and CF). A significant difference in p values of yield stress was observed in (F), represented as ***p value <0.001

Inks	Pressure (kPa)	YS (Pa)	CF (Hz)	G' (Pa)	FD (μm)	Pr value
4% CMC–6% Alg	70	NA	1.6	32 ± 3	310 ± 20	0.82 ± 0.06
4% CMC–8% Alg	145	125 ± 10	NA	132 ± 2	300 ± 40	0.83 ± 0.02
4% CMC–10% Alg	160	388 ± 10	NA	371 ± 3	280 ± 10	0.95 ± 0.08
4% CMC–15% Alg	370	1774 ± 15	NA	1994 ± 5	265 ± 20	0.96 ± 0.02

the ink's visco-elastic solid behavior and no CF (Fig. 2G). As a result, the printed strands could retain the 3D structure (Fig. 2B–D). Also, G' value increased from 32 Pa to 1994 Pa as Alg concentration increased (Table 3). 4% CMC–Alg systems showed the desired rheological properties for printing are: (1) YS above 300 Pa, (2) no CF, (3) $G' > G''$ and in the range of 400 Pa, which is corroborating the conclusions obtained for 4% Alg–**CMC**. 4% CMC–20% Alg was found to be the most desirable formulation from the group based on FD = 255 ± 20 μm and Pr = 1 ± 0.02 values, however the required high printing pressure made it not suitable for bioprinting with cells.

3.3. Printing and rheology of 4% Alg–10% CMC mixed with different concentrations of GelMA (4% Alg–10% CMC–GelMA)

4% Alg–10% CMC, chosen based on 3.1 and 3.2 studies, was combined with 8%, 12%, and 16% GelMA and printed using a metallic cartridge and 200 μm pore diameter metallic nozzle at 37 °C. GelMA was added due to its known biocompatible properties (*i.e.* presence of cell adhesive domains). GelMA is a gelatin-based photo cross-linkable polymer with thermo-responsive properties. Due to the thermoresponsive nature, controlling the printing temperature of 4% Alg–10% CMC–**GelMA** inks was paramount. To minimize the influence of GelMA introduction on the previously optimized ink 4% Alg–10% CMC, the printing temperature was maintained at 37 °C (at this temperature GelMA is a low viscosity liquid).[59] Image analysis of 4% Alg–10% CMC–**GelMA** printed scaffolds showed the Pr value in the range of 0.9 ± 0.01, meaning all the inks could maintain perfect square pores after printing (Table 4). However, FD showed an increase of 5 μm with increasing GelMA concentrations in the inks from 8% to 12% to 16% (Table 4). The increment in fiber diameter was assigned to decreased viscosity and yield stress for 4% Alg–10% CMC–16% GelMA compared to 4% Alg–10% CMC–8% GelMA and 4% Alg–10% CMC–12% GelMA (Fig. 3E and F) at 37 °C. We hypothesize that this caused the strands to collapse when coming in contact with the printing substrate. In conclusion, all the inks with the addition of GelMA were printable.

The flow sweep tests performed at 37 °C corroborate the shear-thinning nature of all inks containing GelMA, with the 4% Alg–10% CMC–16% GelMA sample depicting the lowest viscosity over other inks (Fig. 3G). The amplitude sweep test (Fig. 3F) showed that 4% Alg–10% CMC possesses a higher

Table 4 Summarizes the extrusion pressure, printability quality indices (FD and Pr value), and rheological parameters (YS, G' and CF). A significant difference in p values of yield stress was observed in (F), represented as *p value <0.001

Inks	Pressure (kPa)	YS (Pa)	CF (Hz)	G' (Pa)	FD (μm)	Pr value
4% Alg–10% CMC	200	308 ± 10	NA	487 ± 2	209 ± 10	0.92 ± 0.05
4% Alg–10% CMC–8% GelMA	185	155 ± 25	NA	628 ± 2	210 ± 15	0.95 ± 0.02
4% Alg–10% CMC–12% GelMA	175	142 ± 30	NA	543 ± 3	215 ± 10	0.94 ± 0.05
4% Alg–10% CMC–16% GelMA	165	132 ± 25	NA	564 ± 2	220 ± 10	0.93 ± 0.04

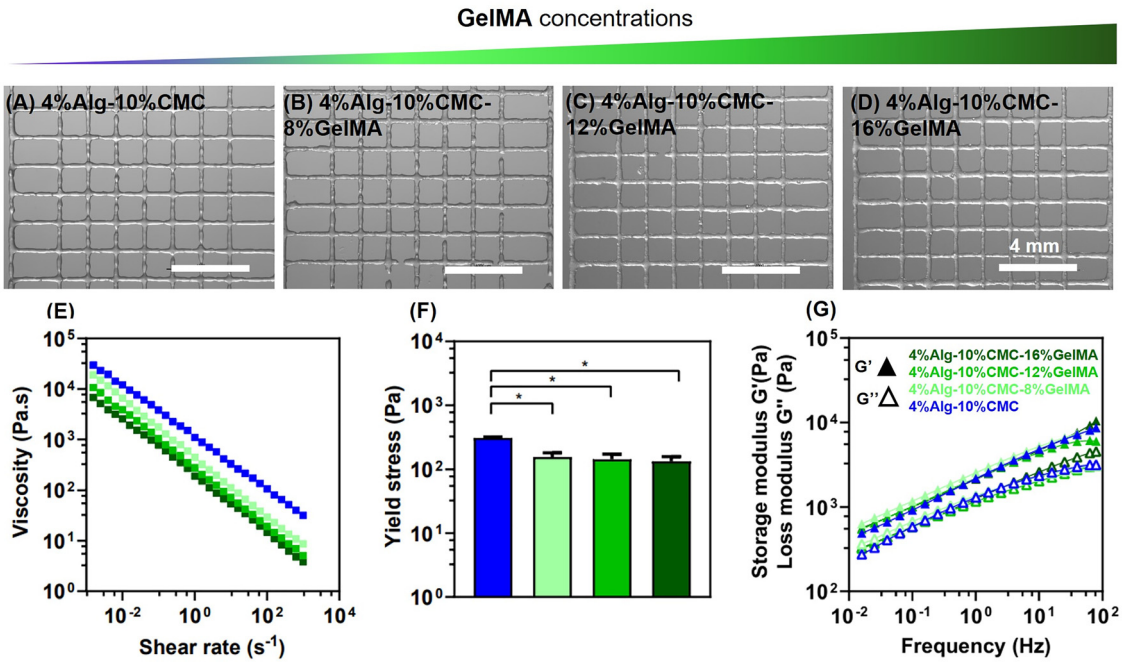

Fig. 3 Correlation between printing and rheology of 4% Alg–10% CMC–**GelMA**. (A)–(D) Represent stereomicroscopic images of 3D-printed scaffolds. (E)–(G) Depict the inks' flow sweep, the yield stress deduced from amplitude sweep and frequency sweep, respectively.

yield stress (308 ± 10 Pa) than 4% Alg–10% CMC–**GelMA**. Among four inks containing GelMA, 4% Alg–10% CMC–16% GelMA showed the lowest yield stress (*i.e.*, 132 ± 25 Pa) compared to 4% Alg–10% CMC with 8% and 12% GelMA having yield stress of 155 ± 25 Pa and 142 ± 30 Pa, respectively. However, the values did not show a significant difference from each other. The G' difference observed among 4% Alg–10% CMC–**GelMA** was reflected in these inks' extrusion pressure and FD values, showing a difference of $\simeq$10 kPa in the pressure and an increase in FD value (Table 3). We assumed that the decrease in yield stress and viscosity value of 4% Alg–10% CMC–**GelMA** samples is caused GelMA at 37 °C interrupting the Alg–CMC network. The frequency sweep test showed no CF for all inks with $G' > G''$ at 37 °C (Fig. 3G). 4% Alg–10% CMC–**GelMA** inks showed a higher G' value than 4% Alg–10% CMC (Table 4). 4% Alg–10% CMC can form an interpenetrating polymeric network with few cross-links, giving rise to a loose network illustrating a lower G' than 4% Alg–10% CMC–**GelMA**. In 4% Alg–10% CMC–**GelMA**, G' increased as GelMA content increased (Table 4).

Based on those results, it can be deduced that to obtain well-printable scaffolds using 4% Alg–10% CMC–**GelMA** material system, the desired rheological properties are: (1) YS above ca 150 Pa (2) no CF, (3) $G' > G''$ and in the range of 600 Pa. Those values are similar to the values observed by us for two other studied systems without GelMA. The optimized bioink not only meets the required quantitative rheological parameters but also supports the fabrication of multilayered, complex 3D structures with excellent shape fidelity and structural integrity—an essential criterion for tissue engineering applications involving large-scale or hierarchically organized constructs (Fig. 5). The following section further studies to determine the apparent shear values experienced by the inks during printing.

3.4. Mathematical modeling of 4% Alg–10% CMC–GelMA

We used the mathematical model reported in eqn (3) to determine the apparent shear rate during printing by knowing the shear thinning exponent and the printing parameters. The apparent viscosity was determined from eqn (2) using apparent shear rate and coefficients, followed by apparent shear stress estimation. This allows us to correlate the magnitude of the shear stress the sample is subjected to during printing to yield stress deduced from the amplitude sweep. The shear viscosity measured in flow sweep (Fig. 3E) showed the ink's resistance to

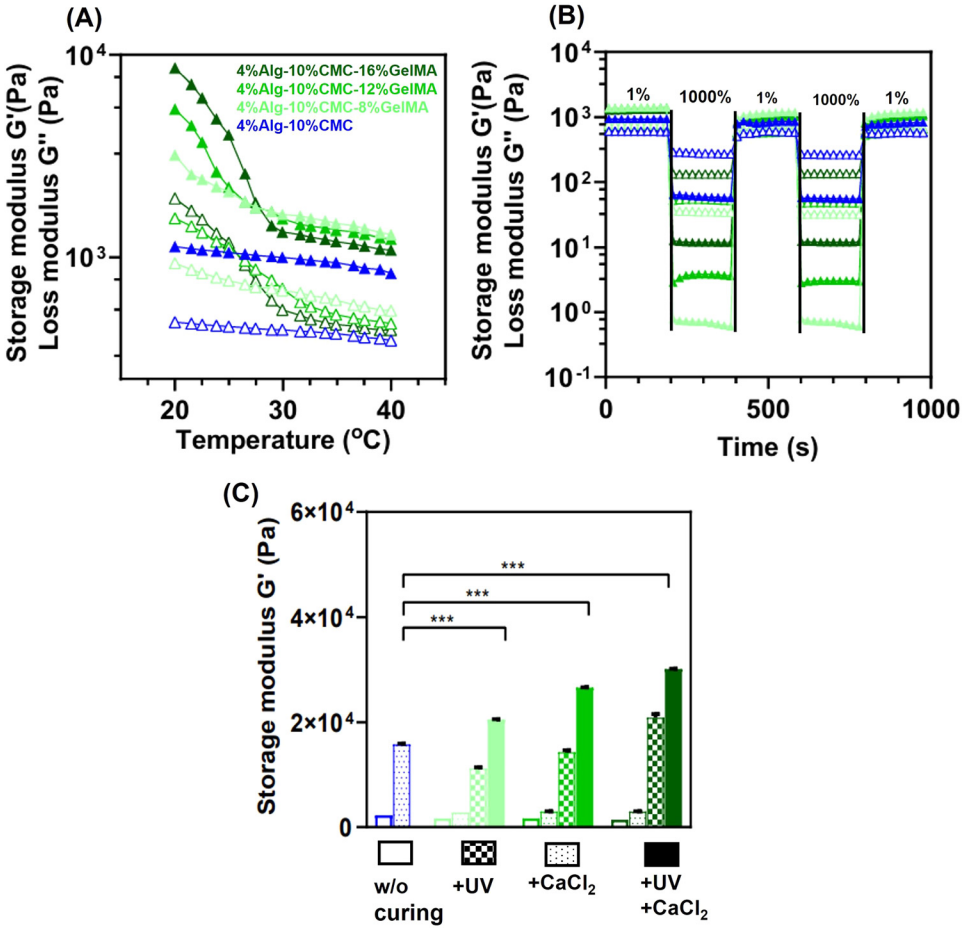

Fig. 4 Temperature ramp, thixotropic test and time sweep tests of 4% Alg–10% CMC–**GelMA**. (A) Temperature ramp, (B) thixotropic test, (C) time sweep test of single ($CaCl_2$ cross-linked and UV cured separately) and dually cross-linked (both $CaCl_2$ cross-linked and UV cured) inks; dually-cured 4% Alg–10% CMC–**GelMA** showed a significant difference in G' compared to $CaCl_2$ cross-linked 4% Alg–10% CMC (***p value < 0.001). The P-value was determined by two-way ANOVA followed by a Tukey multiple comparison *post hoc* test.

flow when the ink is subjected to constant shear rate with varying magnitude, and apparent viscosity during printing conditions defined the shear thinning degree of the formulations. For a shear-thinning ink, n is expected to be less than 1, and the n value quantitively defines the shear-thinning degree (Table 5). The higher the n value of ink, the lower the shear thinning property. 4% Alg–10% CMC depicted $n = 0.5$, meaning it showed the highest n value and least shear thinning nature (Table 4). 4% Alg–10% CMC–**GelMA** inks showed a higher shear thinning nature over 4% Alg–10% CMC due to an increase in the total polymer content of the formulation. Among 4% Alg–10% CMC–**GelMA**, 4% Alg–10% CMC–8% GelMA with n = 0.43 showed the highest shear thinning degree compared to the 4% Alg–10% CMC–12% GelMA and 4% Alg–10% CMC–16% GelMA with n value of 0.44 and 0.46, respectively. In 4% Alg–10% CMC–**GelMA** inks, the shear thinning property decreased with an increase in GelMA content, meaning the presence of GelMA, a thermoresponsive component, lowered the shear thinning nature. Further, the apparent shear stress values of all inks were found to be higher than the yield stress value (Table 5 third column), meaning the ink had to overcome the yield stress to be smoothly extruded during printing.[60] 4% Alg–10% CMC depicted a high yield stress and apparent shear rate value compared to 4% Alg–10% CMC–**GelMA**. However, adding GelMA lowered both values due to GelMA's thermo-responsive nature. The apparent shear rate and shear viscosity experienced by the 4% Alg–10% CMC–**GelMA** inks decreased with increased GelMA, favoring smooth extrudability and cell survivability during printing.

The calculated shear stress and shear viscosity values thus can help predict the maximum stress the cells can tolerate during printing. Studies have shown the shear stress value ranging from 1–10 kPa and shear viscosity value of 1–100 Pa s can employed by extrusion-based bioprinting.[61,62] Another study has proved that shear stress below 4 kPa can help maintain satisfactory mesenchymal stem cell viability during bioprinting.[63] The limit of the apparent shear viscosity and shear stress cells' tolerance depends on the cell type and bioink composition. For instance, human umbilical vein endothelial cells (HUVECs) reported a decreased cell viability due to high shear stress exerted during bio-printing. Shear thinning bioinks containing kappa-carrageenan or silk fibroin help to

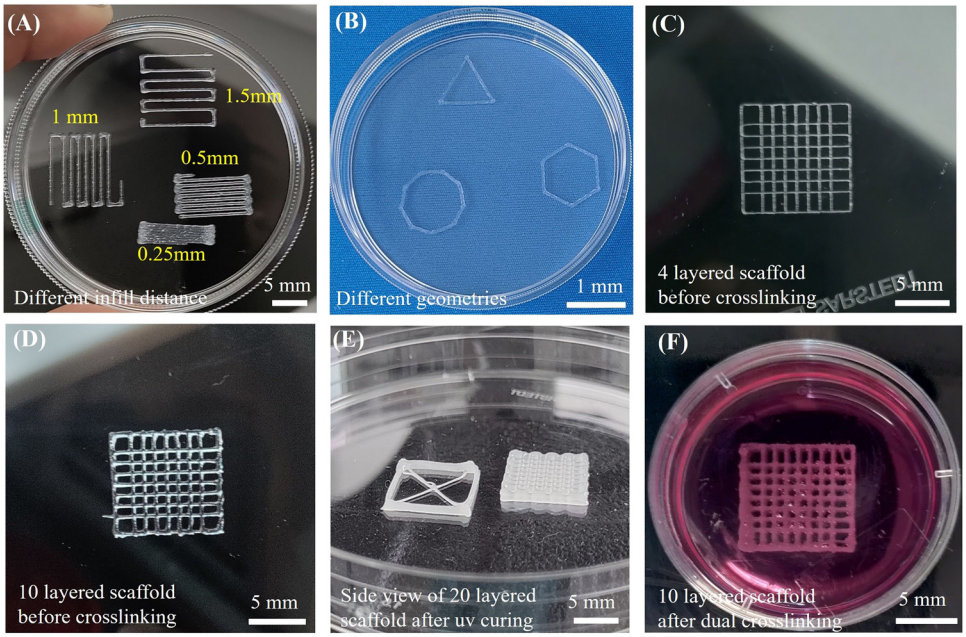

Fig. 5 Macroscopic images of 4% Alg–10% CMC–16% GelMA ink prints to prove its shape fidelity (A) depicts prints in different infill distances (0.25–1.5) mm as marked in the images, (B) represents ink printed in three different geometries (triangle, hexagon and nanogon), (C) and (D) depicts 4 layered and 10 layered scaffolds scaffold (scaffold of 10 × 10 mm dimension and infill distance of 1 mm). (A)–(D) are the images of prints without crosslinking. (E) Depicts side view of 20 layered scaffold after UV curing and (F) illustrates 10 layered scaffold after dual (UV and $CaCl_2$ treatment) crosslinking and incubated in DMEM media with FBS and Pen–Strep for 7 days.

Table 5 Rheological values derived from amplitude sweep for 4% Alg–10% CMC and 4% Alg–10% CMC–GelMA

Different inks	n	Apparent shear rate (s^{-1})	Apparent shear viscosity (Pa s)	Apparent shear stress (Pa)	YS (Pa)
4% Alg–10% CMC	0.5	1316	32.9	43 296	308 ± 10
4% Alg–10% CMC–8% GelMA	0.43	1382	6.9	9535	155 ± 25
4% Alg–10% CMC–12% GelMA	0.44	1273	4.8	6110	142 ± 30
4% Alg–10% CMC–16% GelMA	0.46	1155	4.6	5313	132 ± 25

reduce the stress experienced by the cells during printing.[64,65] In the current study, 4% Alg–10% CMC–**GelMA** inks, with apparent shear stress and shear viscosity in the range of 5313–9535 Pa and 6.9–4.6 Pa s, respectively were found to be suitable for fibroblast survivability, as studied in Section 3.8 (Fig. 6). The obtained values thus quantitatively define the apparent shear stress and viscosity desired to attain a well-printable bioink using 4% Alg–10% CMC–**GelMA** system. Additional rheological studies were performed to analyze the suitability of thermoresponsive ink for printing.

3.5. Temperature ramp, thixotropic, and time sweep of cross-linked 4% Alg–10% CMC–GelMA

Further, a temperature ramp test was performed to analyze the thermo-responsive properties of 4% Alg–10% CMC–**GelMA**. Based on this test, it was observed that 4% Alg–10% CMC–**GelMA** showed a gradual decrease in G' value with an increase in temperature, and the values did not significantly differ from 35 °C to 40 °C (Fig. 4A). Due to the non-thermo responsive nature of Alg and CMC, the control (4% Alg–10% CMC) showed a lower G' value than 4% Alg–10% CMC–**GelMA**, but G' did not show variation at different temperatures. The temperature ramp was performed at a frequency of 0.1 rad s^{-1}. The test is frequency-dependent, and the modulus value would differ based on the chosen frequency. This statement can be proved based on the frequency sweep test, which showed an increase in modulus value with an increase in frequency (Fig. 3G). Comparing the G' values at 37 °C, 4% Alg–10% CMC–16% **GelMA** revealed a lower G' value (1136 ± 30 Pa) than 4% Alg–10% CMC with 8% and 12% GelMA with a G' value of 1400 ± 25 Pa and 1300 ± 25 Pa, respectively (Fig. 4A).

To verify the effect of printing temperature on 4% Alg–10% CMC with 8% and 12% GelMA and how it differed between the two inks, the inks were printed at 25 °C and 37 °C (Fig. S11). At 25 °C, the G' value of 4% Alg–10% CMC–8% GelMA and 4% Alg–10% CMC–12% GelMA were found to be 5372 ± 10 Pa and 8196 ± 10 Pa, respectively (Fig. 4A). When printing these inks at 25 °C, 4% Alg–10% CMC–12% GelMA with higher G' value showed better printability (Pr = 0.98 ± 0.02 and FD = 200 ± 20 μm) demanding higher printing pressure (400 kPa) compared

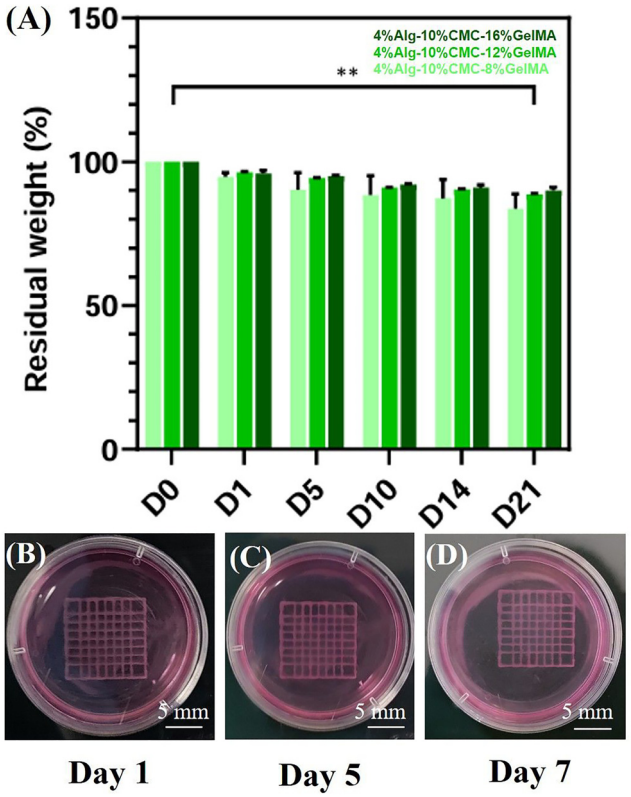

Fig. 6 Post-printing stability/degradability of 4% Alg–10% CMC–**GelMA** constructs: (A) a graphical representation of 3D printed scaffold stability (without cells) over 21 days, illustrating changes in residual weight from day 0 to day 21 (**p value <0.05). The P-value was determined by two-way ANOVA followed by a Tukey multiple comparison *post hoc* test. The color of the bar graph represents the 4% Alg–10% CMC–**GelMA** formulation, as defined in Fig. 4. (B)–(D) Macroscopic images of 4-layered 3D bioprinted scaffolds (4% Alg–10% CMC–16% GelMA) captured on days 1, 5, and 7, showing clear shape retention and confirming structural integrity during culture.

to 4% Alg–10% CMC–8%GelMA (Pr = 0.98 ± 0.01 and FD = 205 ± 20 μm) and printing at a pressure of 300 kPa (Fig. S11). A lower G' value was observed for 4% Alg–10% CMC–12% GelMA than 4% Alg–10% CMC–8% GelMA. These results are incongruent with the printing results at 37 °C, which proved 4% Alg–10% CMC–12% GelMA to give better prints, with Pr = 0.95 ± 0.02 and FD = 210 ± 10 μm at a pressure of 175 kPa compared to 4% Alg–10% CMC–8% GelMA giving prints (with Pr = 0.94 ± 0.05 and FD = 215 ± 10 μm) at 180 kPa. The above test proved that at a lower temperature (25 °C), 4% Alg–10% CMC with 8% and 12% GelMA inks showed a higher G' value demanding higher extrusion pressure at 37 °C. Printing of 4% Alg–10% CMC with 8%, 12% and 16% GelMA was performed at 30 °C and 37 °C (Fig. S12), which also showed the same trend, proving the dependency of GelMA content on the printing temperature. Based on these results, 37 °C was chosen as the printing temperature as it enables smooth extrudability of cell-encapsulated ink with minimal shear, easing cell survival. This is also the most beneficial temperature maintaining high cell viability and cell culture.

The thixotropic test for 4% Alg–10% CMC and 4% Alg–10% CMC–**GelMA** at 37 °C was performed to mimic pre-, during, and post-printing conditions. It was observed that all the inks seem to depict a visco-elastic solid behavior ($G' > G''$) at minimal strain (1%), mimicking the pre-printing condition, ($G'' > G'$) at maximal strain (1000%) mimicking printing process, and full recovery after increased strain removal (back to 1%) (Fig. 4B). The test thus proved the self-healing or structural recovery of the inks when subjected to varying strains.

To determine the final stiffness of all the material systems in single and dual cross-linking conditions (UV curing and $CaCl_2$ cross-linking), the G' value was derived using a time sweep performed at 1% strain and 0.1 rad s^{-1} angular frequency. 4% Alg–10% CMC ink showed a significant increase in G' to 15 754 ± 200 Pa after $CaCl_2$ with respect to the untreated sample with G' of 2269 ± 5 Pa. 4% Alg–10% CMC with 8%,12% and 16% GelMA control without any cross-linking depicted G' values of 1672 ± 3, 1562 ± 5, and 1415 ± 7, respectively (Fig. 4C). G' value after $CaCl_2$ cross-linking increased further to 2774 ± 40, 2971 ± 51 and 2977 ± 63 Pa, respectively. $CaCl_2$ cross-linked 4% Alg–10% CMC–**GelMA** inks did not show any significant difference in G' value among themselves. We assigned this result to the unavailability of the carboxyl group of Alg for Ca^{2+} binding, which is involved in an electrostatic interaction with the amine group of GelMA.[66]

Irradiation with UV at a power of 25 mW cm^{-2} for 1 min showed an improvement in the G' value of 4% Alg–10% CMC–**GelMA**, depending on GelMA concentration. After UV curing, G' value of 4% Alg–10% CMC–(8,12,16)% GelMA reached 11 218 ± 182, 14 303 ± 350, and 20 892 ± 685 Pa, respectively (Fig. 4C). It can inferred that after UV curing, G' value significantly increased with an increase in GelMA content. The increase in G' with GelMA content is due to a high methacryloyl group available on GelMA, which enhances the cross-linking density and G' values.

On comparing G' values of single cross-linked 4% Alg–10% CMC–**GelMA** with dually cured 4% Alg–10% CMC–**GelMA**, it was observed that the inks showed a significant difference to each other ($p < 0.001$). Dually cured 4% Alg–10% CMC–**GelMA** inks also showed G' values of 20 544 ± 43, 26 576 ± 27, and 30 132 ± 35 Pa, respectively, illustrating a difference of approximately 5000 Pa to each other ($p < 0.001$). Among 4% Alg–10% CMC–**GelMA**, 4% Alg–10% CMC–16% GelMA showed the highest G' compared to 4% Alg–10% CMC with 8% and 12% GelMA. Thus, it can be inferred that stiffness can be adjusted based on GelMA content. The cross-linking was not performed in the reverse order (first $CaCl_2$ cross-linking followed by UV curing) because it could potentially result in photo-initiator (LAP) leakage during $CaCl_2$ incubation, reducing UV curing efficiency.

A temperature ramp of dual-cured 4% Alg–10% CMC–**GelMA** inks was also performed, and showed G' and G'' to be constant at different temperatures (Fig. S2). This proved that the inks did not respond to the temperature change after dual curing anymore. The results, therefore, show the dual-cured scaffold would not demonstrate any change in stiffness (G' value) in culturing conditions of 37 °C.

Each rheological test provides crucial information on the desirable properties that make the inks suitable for bioprinting applications. It is recommended to perform the tests in the order: flow sweep, oscillation tests, and thixotropic tests, followed by other modifications of the oscillation test to study the change in the ink's nature depending on specific stimuli (like temperature and uv curing). The congruency of the rheological result with printing quality indices affirms that rheological testing can ease bioink design. The rheological parameters and conditions must be chosen considering what information has to be deduced and how this information will be employed in future steps. For instance, the rheological testing of 4% Alg–10% CMC–**GelMA** at 37 °C is paramount as the gel properties would differ at various temperatures due to GelMA's gelation. The resulting difference in viscosity and yield stress is essential to predict the survival of cells during printing. Another example is the dual cross-linking test, which proved the plausibility of using the dual-cured 3D-printed 4% Alg–10% CMC–**GelMA** inks to generate a gradient system with a difference in final stiffness. Therefore, apart from identifying the fundamental rheological properties of bioink, the test should be performed while considering the end goal of the inks.

3.6. Shape fidelity assessment in complex 3D constructs

To assess the structural performance of the optimized 4% Alg–10% CMC–16% GelMA ink, a series of constructs was printed to evaluate its shape fidelity, spatial resolution, and structural stability. Constructs with varying infill distances (0.25–1.5 mm) were successfully fabricated (Fig. 5A), showing clearly separated and well-defined strands across all spacings. This confirmed the ink's ability to support fine resolution and spatial control, even in the pre-crosslinked state. Additionally, the ink maintained shape fidelity in more complex geometries, including triangles, hexagons, and irregular polygons (Fig. 5B), further demonstrating its precision during extrusion. Multi-layered printing tests revealed that both 4-layer and 10-layer grid scaffolds remained self-supporting before crosslinking, indicating a non-collapsing nature (Fig. 5C and D). Post-crosslinking performance was evaluated through a 20-layer construct, which retained its vertical structure and layer resolution after UV curing (Fig. 5E), verifying the effectiveness of photopolymerization in stabilizing the architecture. Finally, to assess long-term mechanical stability in a biological environment, a 10-layer construct was dual-crosslinked (UV and calcium chloride) and incubated in DMEM for 7 days. The scaffold exhibited no signs of deformation or degradation (Fig. 5F), indicating stability of multilayered constructs.

Overall, these results validate the robustness of the optimized bioink in supporting complex, multilayered 3D constructs. The ink exhibited excellent shape fidelity across various geometries, structural integrity in the non-crosslinked state, and sustained stability under physiological conditions. This highlights the bioink's potential for use in tissue engineering applications where both architectural precision and long-term mechanical durability are critical.

3.7. Post-printing stability/degradability of 3D printed 4% Alg–10% CMC–GelMA constructs

3D-printed dually cured 4% Alg–10% CMC–**GelMA** scaffolds were incubated in DMEM media supplemented with FBS and Pen–Strep at 37 °C to check the stability of the scaffolds. The weight of the scaffolds was taken to calculate the residual weight of the samples. The scaffolds with 4% Alg–10% CMC with 8%,12% and 16% GelMA after 21 days of incubation showed a residual weight of 83%, 88%, and 90%, respectively (Fig. 6A). The results showed that dually-cured 4% Alg–10% CMC–**GelMA** scaffolds could maintain their structural integrity until day 21. Meanwhile, scaffolds printed with 4% Alg–10% CMC ink (without GelMA) could not maintain their structure and were dissolved in the media in less than 24 hours. The electrostatically bonded Alg/CMC/GelMA polymers, after a dually cross-linking process with non-covalently bonded Alg–Ca and an irreversible covalent bonded photo-cross-linked GelMA keeps the Alg/CMC/GelMA network intact with slow degradation property. To qualitatively support the degradation study, macroscopic evaluation of 4-layered 3D bio-printed 4% Alg–10% CMC–16% GelMA over 7 days in culture was performed. Structural fidelity and a defined pore architecture were maintained throughout the 7-day period, indicating the long-term stability of 3DBP constructs (Fig. 6B–D). The stability study results proved that the 3D-printed scaffolds generated using optimized inks possess handling properties, maintain shape, and can be used for further cell studies.

3.8. Biocompatibility of 3D bioprinted 4% Alg–10% CMC–GelMA

Biocompatibility and estimation of cell viability of 3D bioprinted 4% Alg–10% CMC–(8,12,16)% GelMA was performed using a live–dead assay and an Alamar blue assay. Temperature control during cell mixing and order of bioink component mixing, specifically maintaining the ink at 37 °C, is vital as it minimizes shear stress and mixing time and enables more uniform cell incorporation compared to preparation without temperature regulation (as demonstrated in Fig. S15 and S16).

The live–dead assay results showed that the cells were alive in all inks. However, they were round in shape. As the culturing days increased and the live cell number increased, the cells started to show an elongated morphology (Fig. 7A–I). The Alamar blue results quantitatively supported the live–dead test based on the percentage of reduced Alamar blue. 4% Alg–10% CMC–(8,12,16)% GelMA constructs demonstrated a 10%, 20%, and 40% increase in cell metabolic activity, respectively, from day 1 to day 7 of culture (Fig. 7J). These observations can be traced to the previous studies that proved higher fibroblast spreading in the 3D printed GelMA hydrogel with matrix stiffness greater than 20 kPa.[67,68]

The increase in cell metabolic activity with increased GelMA concentration in the inks could also be associated with the presence of the cell adhesion (RGD) domains. The combination of the higher amount of RGDs and increased stiffness proved the 3D bio-printed 4% Alg–10% CMC–**GelMA** scaffolds to have excellent biocompatibility.

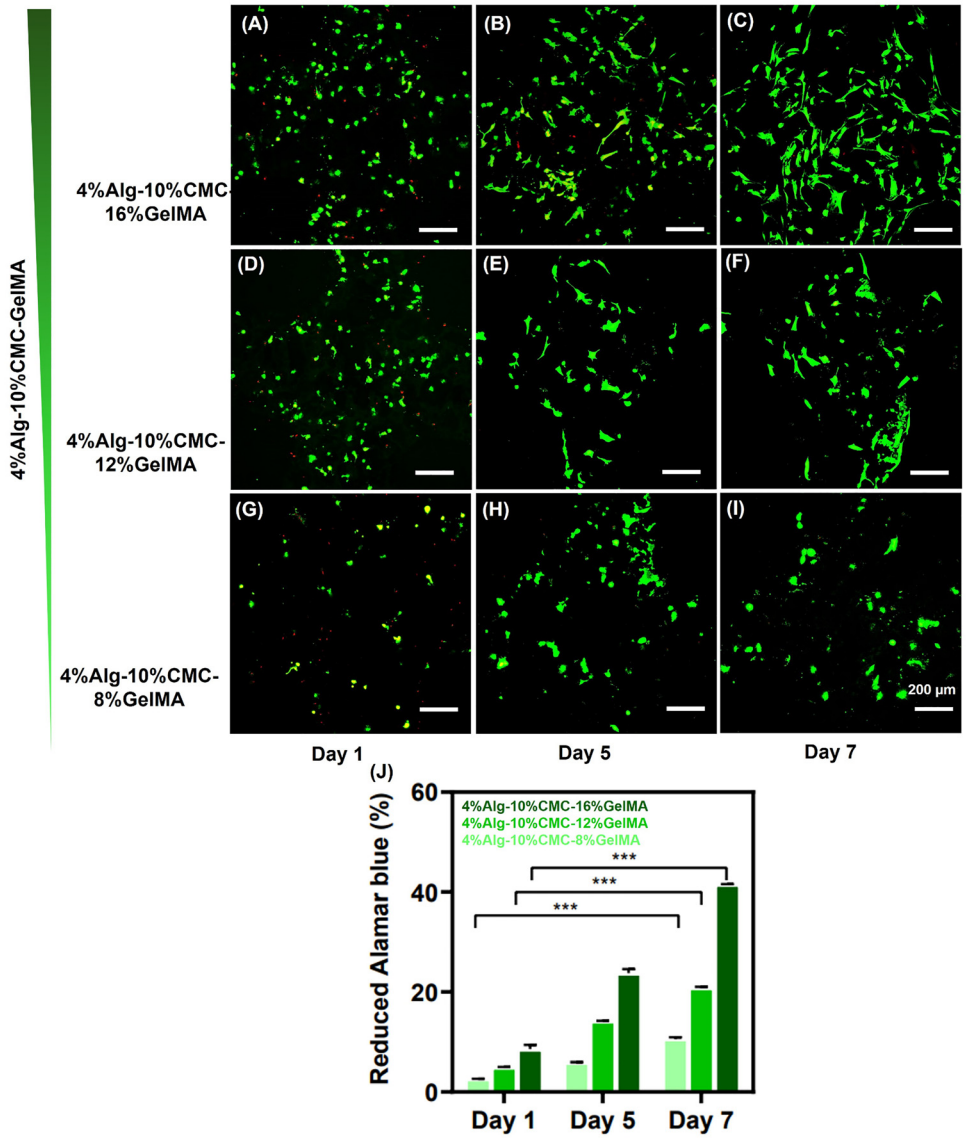

Fig. 7 Biocompatibility evaluation of 4% Alg–10% CMC–**GelMA**: live–dead assay (A)–(I) and Alamar blue assay (J) of 4% Alg–10% CMC with 8%, 12% and 16% GelMA for day 1, 5, and 7 of culturing. Scale bars: 200 μm (***p-value <0.001).

Various attempts have been initiated using the Alg/GelMA combination for numerous tissue engineering applications.[50,69,70] Also, previous studies have proven the fabrication of a tri-composite Alg/CMC/gelatin scaffold for human meniscus knee regeneration and 3D printed Alg/CMC constructs as a potential scaffold in tissue engineering.[48,66] However, no studies are currently available that have employed dually cured Alg/CMC/GelMA ink in 3D bio-printing applications. 4% Alg–10% CMC–**GelMA** inks proved to have more stability with residual weight (of an average of 87%) on day 21 compared to the Alg/CMC/gelatin scaffold[56] that demonstrated a 50% weight loss of the scaffolds on day 25.[66] Among 4% Alg–10% CMC–**GelMA**, 4% Alg–10% CMC–16% GelMA ink was observed to show best printability with desirable rheological properties, scaffold stability, and excellent biocompatibility. However, 4% Alg–10% CMC–(8,12)% GelMA inks also seem to be promising. The combination of all testes 4% Alg–10% CMC–**GelMA** inks can be employed for the regeneration of gradient or interface tissue, such as myotendinous or muscle-skeletal engineering.

4. Conclusions

This study presents a comprehensive framework for designing dually cured Alg/CMC/GelMA bioinks that optimize printability, scaffold stability, and biocompatibility. By correlating rheological parameters such as yield stress (YS), cross-over frequency (CF) and G' with printability quality indices (fiber diameter, FD, and printability value, Pr) and extrusion pressure, it establishes quantitative guidelines for achieving optimally printable formulations.

Importantly, the mechanical tunability of the bioink optimized in this study falls within the ideal range reported for successful tissue engineering applications, exhibiting storage moduli between approximately 200–500 Pa which supports smooth extrusion and reliable shape retention, while preserving high cell viability.[71] While previous studies on GelMA or alginate-based systems report similar modulus ranges, the novelty of our approach lies in integrating a structured validation of printability, biocompatibility, and long-term culture stability, offering a robust and adaptable strategy for developing bioinks suitable for complex, multilayered tissue constructs.

Despite the well-documented relationship between rheology and printing, this study fills a critical gap by providing a systematic protocol linking these parameters. For Alg–CMC inks the desired rheological properties for printing are: (1) YS above 300 Pa, (2) no CF, (3) $G' > G''$ and in the range of 400 Pa. While in case of 4% Alg–10% CMC–**GelMA** inks (1) YS above ca 150 Pa (2) no CF, (3) $G' > G''$ and in the range of 600 Pa are beneficial, allowing good printability at pressures suitable for printing with cells. Our results also indicates that for these inks the apparent shear stress and viscosity in the range of 5000–9500 Pa and 5–7 Pa s, respectively, ensure mild printing conditions supportive cells viability after extrusion. This study also identifies 4% Alg–10% CMC as superior to 4% CMC–Alg due to the collapsing nature of Alg when used as a primary component. Adjusting the emulsifier concentration (CMC) proved more effective for achieving optimal rheological and printing properties. Rheological tests pinpointed 37 °C as the optimal printing temperature for the 4% Alg–10% CMC–**GelMA** system, reducing thermal stress on cells and enhancing bioprinting efficiency. The final range of scaffold stiffness values highlights the potential for applications in graded tissue regeneration, validated by stability and biocompatibility testing.

This approach offers a practical and reproducible protocol that can be adapted to other multi-component hydrogel systems, enabling researchers to tune their bioink composition for extrusion-based bioprinting applications rationally. By defining the optimal rheological and printability parameters for bioink development, this study sets a benchmark for future research, offering critical insights for advancing extrusion-based bioprinting applications.

Conflicts of interest

The authors affirm that they have no conflicts of interest to disclose.

Data availability

The data supporting the findings of this study can be obtained from the corresponding author upon reasonable request.

Supplementary information is available. See DOI: **https://doi.org/10.1039/d5tb00737b**.

Acknowledgements

R. G., J. Z.-P. and M. K. W.-B. gratefully acknowledge financial support from the Polish National Agency for Academic Exchange (NAWA, Polish Returns grant no. PPN/PPO/2019/1/00004/U/0001) and the National Science Centre, Poland (NCN, OPUS grant no. 2020/37/B/ST5/00743).

References

1 I. Matai, G. Kaur, A. Seyedsalehi, A. McClinton and C. T. Laurencin, Progress in 3D Bioprinting Technology for Tissue/Organ Regenerative Engineering, *Biomaterials*, 2020, **226**, 119536, DOI: **10.1016/J.BIOMATERIALS.2019.119536**.

2 P. S. Zieliński, P. K. R. Gudeti, T. Rikmanspoel and M. K. Włodarczyk-Biegun, 3D Printing of Bio-Instructive Materials: Toward Directing the Cell, *Bioact. Mater.*, 2023, **19**, 292–327, DOI: **10.1016/J.BIOACTMAT.2022.04.008**.

3 B. Tan, S. Gan, X. Wang, W. Liu and X. Li, Applications of 3D Bioprinting in Tissue Engineering: Advantages, Deficiencies, Improvements, and Future Perspectives, *J. Mater. Chem. B*, 2021, **9**(27), 5385–5413, DOI: **10.1039/D1TB00172H**.

4 M. Mirshafiei, H. Rashedi, F. Yazdian, A. Rahdar and F. Baino, Advancements in Tissue and Organ 3D Bioprinting: Current Techniques, Applications, and Future Perspectives, *Mater. Des.*, 2024, **240**, 112853, DOI: **10.1016/J.MATDES.2024.112853**.

5 J. Karvinen and M. Kellomäki, Design Aspects and Characterization of Hydrogel-Based Bioinks for Extrusion-Based Bioprinting, *Bioprinting*, 2023, **32**, e00274, DOI: **10.1016/J.BPRINT.2023.E00274**.

6 S. H. Kim, Y. K. Yeon, J. M. Lee, J. R. Chao, Y. J. Lee, Y. B. Seo, M. T. Sultan, O. J. Lee, J. S. Lee, S. Il Yoon, I. S. Hong, G. Khang, S. J. Lee, J. J. Yoo and C. H. Park, Precisely Printable and Biocompatible Silk Fibroin Bioink for Digital Light Processing 3D Printing, *Nat. Commun.*, 2018, **9**(1), 1–14, DOI: **10.1038/s41467-018-03759-y**.

7 W. Long Ng, V. Shkolnikov, B. Wei Long Ng and B. Viktor Shkolnikov, Jetting-Based Bioprinting: Process, Dispense Physics, and Applications, *Bio-Des. Manuf.*, 2024, **7**(5), 771–799, DOI: **10.1007/S42242-024-00285-3**.

8 R. Levato, O. Dudaryeva, C. E. Garciamendez-Mijares, B. E. Kirkpatrick, R. Rizzo, J. Schimelman, K. S. Anseth, S. Chen, M. Zenobi-Wong and Y. S. Zhang, Light-Based Vat-Polymerization Bioprinting, *Nat. Rev. Methods Primers*, 2023, **3**(1), 1–19, DOI: **10.1038/s43586-023-00231-0**.

9 J. Groll, J. A. Burdick, D. W. Cho, B. Derby, M. Gelinsky, S. C. Heilshorn, T. Jüngst, J. Malda, V. A. Mironov, K. Nakayama, A. Ovsianikov, W. Sun, S. Takeuchi, J. J. Yoo and T. B. F. Woodfield, A Definition of Bioinks and Their Distinction from Biomaterial Inks, *Biofabrication*, 2018, **11**(1), 013001, DOI: **10.1088/1758-5090/AAEC52**.

10 E. Mancha Sánchez, J. C. Gómez-Blanco, E. López Nieto, J. G. Casado, A. Macías-García, M. A. Díaz Díez, J. P. Carrasco-Amador, D. Torrejón Martín, F. M. Sánchez-Margallo and J. B. Pagador, Hydrogels for Bioprinting:

A Systematic Review of Hydrogels Synthesis, Bioprinting Parameters, and Bioprinted Structures Behavior, *Front. Bioeng. Biotechnol.*, 2020, **8**, 541593, DOI: **10.3389/FBIOE.2020.00776/BIBTEX**.

11 S. Raees, F. Ullah, F. Javed, H. M. Akil, M. Jadoon Khan, M. Safdar, I. U. Din, M. A. Alotaibi, A. I. Alharthi, M. A. Bakht, A. Ahmad and A. A. Nassar, Classification, Processing, and Applications of Bioink and 3D Bioprinting: A Detailed Review, *Int. J. Biol. Macromol.*, 2023, **232**, 123476, DOI: **10.1016/J.IJBIOMAC.2023.123476**.

12 S. Naghieh and X. Chen, Printability–A Key Issue in Extrusion-Based Bioprinting, *J. Pharm. Anal.*, 2021, **11**(5), 564–579, DOI: **10.1016/j.jpha.2021.02.001**.

13 E. Monferrer, S. Martín-Vañó, A. Carretero, A. García-Lizarribar, R. Burgos-Panadero, S. Navarro, J. Samitier and R. Noguera, A Three-Dimensional Bioprinted Model to Evaluate the Effect of Stiffness on Neuroblastoma Cell Cluster Dynamics and Behavior, *Sci. Rep.*, 2020, **10**(1), 1–12, DOI: **10.1038/s41598-020-62986-w**.

14 D. Venkata Krishna and M. Ravi Sankar, Persuasive Factors on the Bioink Printability and Cell Viability in the Extrusion-Based 3D Bioprinting for Tissue Regeneration Applications, *Eng. Regen.*, 2023, **4**(4), 396–410, DOI: **10.1016/J.ENGREG.2023.07.002**.

15 S. Kyle, Z. M. Jessop, A. Al-Sabah and I. S. Whitaker, ''Printability'' of Candidate Biomaterials for Extrusion Based 3D Printing: State-of-the-Art, *Adv. Healthcare Mater.*, 2017, **6**(16), 1700264, DOI: **10.1002/ADHM.201700264**.

16 S. Mypati, A. Docoslis and D. P. J. Barz, Direct Writing of Liquids by Micro Dispensing: Stability and Shape of Laminar Jets with High Froude Numbers, *Chem. Eng. J.*, 2020, **381**, 122645, DOI: **10.1016/J.CEJ.2019.122645**.

17 Z. Zhang, Y. Jin, J. Yin, C. Xu, R. Xiong, K. Christensen, B. R. Ringeisen, D. B. Chrisey and Y. Huang, Evaluation of Bioink Printability for Bioprinting Applications, *Appl. Phys. Rev.*, 2018, **5**(4), 41304, DOI: **10.1063/1.5053979/13188892/041304_1_ACCEPTED_MANUSCRIPT.PDF**.

18 D. A. Rau, C. B. Williams and M. J. Bortner, Rheology and Printability: A Survey of Critical Relationships for Direct Ink Write Materials Design, *Prog. Mater. Sci.*, 2023, **140**, 101188, DOI: **10.1016/J.PMATSCI.2023.101188**.

19 P. A. Amorim, M. A. d'Ávila, R. Anand, P. Moldenaers, P. Van Puyvelde and V. Bloemen, Insights on Shear Rheology of Inks for Extrusion-Based 3D Bioprinting, *Bioprinting*, 2021, **22**, e00129, DOI: **10.1016/J.BPRINT.2021.E00129**.

20 A. J. Seymour, A. D. Westerfield, V. C. Cornelius, Z. Li, A. Ramos, M.-C. Li, N. Paxton, W. Smolan, T. Böck, F. Melchels, J. Groll and T. Jungst, Proposal to Assess Printability of Bioinks for Extrusion-Based Bioprinting and Evaluation of Rheological Properties Governing Bioprintability, *Biofabrication*, 2017, **9**(4), 044107, DOI: **10.1088/1758-5090/AA8DD8**.

21 J. D. Ferry, *Viscoelastic Properties of Polymers*, 1980, DOI: **10.1149/1.2428174**.

22 M. Zhang, J. He, M. Deng, P. Gong, X. Zhang, M. Fan and K. Wang, Rheological Behaviours of Guar Gum Derivatives with Hydrophobic Unsaturated Long-Chains, *RSC Adv.*, 2020, **10**(53), 32050, DOI: **10.1039/D0RA04322B**.

23 R. A. Mohamed Yunus and D. Parisi, Scaling Laws in Polysaccharide Rheology: Comparative Analysis of Water and Ionic Liquid Systems, *Biomacromolecules*, 2024, **25**, 6883–6898, DOI: **10.1021/ACS.BIOMAC.4C01125/ASSET/IMAGES/LARGE/BM4C01125_0008.JPEG**.

24 A. L. Lima, F. Q. Pires, L. A. Hilgert, L. L. Sa-Barreto, T. Gratieri, G. M. Gelfuso and M. Cunha-Filho, Oscillatory Shear Rheology as an In-Process Control Tool for 3D Printing Medicines Production by Fused Deposition Modeling, *J. Manuf. Process.*, 2022, **76**, 850–862, DOI: **10.1016/J.JMAPRO.2022.03.001**.

25 D. L. Taylor and M. In Het Panhuis, Self-Healing Hydrogels, *Adv. Mater.*, 2016, **28**(41), 9060–9093, DOI: **10.1002/ADMA.201601613**.

26 M. Shin, S. H. Shin, M. Lee, H. J. Kim, J. H. Jeong, Y. H. Choi, D. X. Oh, J. Park, H. Jeon and Y. Eom, Rheological Criteria for Distinguishing Self-Healing and Non-Self-Healing Hydrogels, *Polymer*, 2021, **229**, 123969, DOI: **10.1016/J.POLYMER.2021.123969**.

27 T. Gao, G. J. Gillispie, J. S. Copus, A. P. R. Kumar, Y. J. Seol, A. Atala, J. J. Yoo and S. J. Lee, Optimization of Gelatin–Alginate Composite Bioink Printability Using Rheological Parameters: A Systematic Approach, *Biofabrication*, 2018, **10**(3), 034106, DOI: **10.1088/1758-5090/AACDC7**.

28 A. Pössl, D. Hartzke, T. M. Schmidts, F. E. Runkel and P. Schlupp, A Targeted Rheological Bioink Development Guideline and Its Systematic Correlation with Printing Behavior, *Biofabrication*, 2021, **13**(3), 035021, DOI: **10.1088/1758-5090/ABDE1E**.

29 G. J. Gillispie, J. Copus, M. Uzun-Per, J. J. Yoo, A. Atala, M. K. K. Niazi and S. J. Lee, The Correlation between Rheological Properties and Extrusion-Based Printability in Bioink Artifact Quantification, *Mater. Des.*, 2023, **233**, 112237, DOI: **10.1016/J.MATDES.2023.112237**.

30 A. Ribeiro, M. M. Blokzijl, R. Levato, C. W. Visser, M. Castilho, W. E. Hennink, T. Vermonden and J. Malda, Assessing Bioink Shape Fidelity to Aid Material Development in 3D Bioprinting, *Biofabrication*, 2017, **10**(1), 014102, DOI: **10.1088/1758-5090/AA90E2**.

31 M. K. Włodarczyk-Biegun, J. I. Paez, M. Villiou, J. Feng and A. Del Campo, Printability Study of Metal Ion Crosslinked PEG-Catechol Based Inks, *Biofabrication*, 2020, **12**(3), 035009, DOI: **10.1088/1758-5090/AB673A**.

32 X. Li, J. Ren, Y. Huang, L. Cheng and Z. Gu, Applications and Recent Advances in 3D Bioprinting Sustainable Scaffolding Techniques, *Molecules*, 2025, **30**(14), 3027, DOI: **10.3390/MOLECULES30143027**.

33 Z. Wu, X. Su, Y. Xu, B. Kong, W. Sun and S. Mi, Bioprinting Three-Dimensional Cell-Laden Tissue Constructs with Controllable Degradation, *Sci. Rep.*, 2016, **6**(1), 1–10, DOI: **10.1038/srep24474**.

34 Z. Ge, Z. Jin and T. Cao, Manufacture of Degradable Polymeric Scaffolds for Bone Regeneration, *Biomed. Mater.*, 2008, **3**(2), 022001, DOI: **10.1088/1748-6041/3/2/022001**.

35 S. Naghieh, M. R. Karamooz-Ravari, M. D. Sarker, E. Karki and X. Chen, Influence of Crosslinking on the Mechanical Behavior of 3D Printed Alginate Scaffolds: Experimental and Numerical Approaches, *J. Mech. Behav. Biomed. Mater.*, 2018, **80**, 111–118, DOI: 10.1016/J.JMBBM.2018.01.034.

36 R. Roque, G. F. Barbosa and A. C. Guastaldi, Design and 3D Bioprinting of Interconnected Porous Scaffolds for Bone Regeneration. An Additive Manufacturing Approach, *J. Manuf. Process.*, 2021, **64**, 655–663, DOI: 10.1016/J.JMAPRO.2021.01.057.

37 A. Schwab, R. Levato, M. D'Este, S. Piluso, D. Eglin and J. Malda, Printability and Shape Fidelity of Bioinks in 3D Bioprinting, *Chem. Rev.*, 2020, **120**(19), 11028–11055, DOI: 10.1021/ACS.CHEMREV.0C00084/ASSET/IMAGES/LARGE/CR0C00084_0009.JPEG.

38 C. Kucukgul, S. B. Ozler, I. Inci, E. Karakas, S. Irmak, D. Gozuacik, A. Taralp and B. Koc, 3D Bioprinting of Biomimetic Aortic Vascular Constructs with Self-Supporting Cells, *Biotechnol. Bioeng.*, 2015, **112**(4), 811–821, DOI: 10.1002/BIT.25493.

39 X. Wang, Q. Ao, X. Tian, J. Fan, H. Tong, W. Hou and S. Bai, Gelatin-Based Hydrogels for Organ 3D Bioprinting, *Polymers*, 2017, **9**(9), 401, DOI: 10.3390/POLYM9090401.

40 D. J. Choi, Y. J. Kho, S. J. Park, Y. J. Kim, S. Chung and C. H. Kim, Effect of Cross-Linking on the Dimensional Stability and Biocompatibility of a Tailored 3D-Bioprinted Gelatin Scaffold, *Int. J. Biol. Macromol.*, 2019, **135**, 659–667, DOI: 10.1016/J.IJBIOMAC.2019.05.207.

41 M. K. Dey and R. V. Devireddy, Rheological Characterization and Printability of Sodium Alginate–Gelatin Hydrogel for 3D Cultures and Bioprinting, *Biomimetics*, 2025, **10**(1), 28, DOI: 10.3390/BIOMIMETICS10010028.

42 A. Khavari, M. Nydén, D. A. Weitz and A. J. Ehrlicher, Composite Alginate Gels for Tunable Cellular Microenvironment Mechanics, *Sci. Rep.*, 2016, **6**(1), 1–11, DOI: 10.1038/SREP30854;TECHMETA=14;SUBJMETA=2268,301,54,57,631,639;KWRD=BIOMATERIALS,BIOPOLYMERS+IN+VIVO.

43 J. He, Y. Sun, Q. Gao, C. He, K. Yao, T. Wang, M. Xie, K. Yu, J. Nie, Y. Chen and Y. He, Gelatin Methacryloyl Hydrogel, from Standardization, Performance, to Biomedical Application, *Adv. Healthcare Mater.*, 2023, **12**(23), 2300395, DOI: 10.1002/ADHM.202300395;REQUESTEDJOURNAL:JOURNAL:21922659.

44 Y. Zhu, X. Yu, H. Liu, J. Li, M. Gholipourmalekabadi, K. Lin, C. Yuan and P. Wang, Strategies of Functionalized GelMA-Based Bioinks for Bone Regeneration: Recent Advances and Future Perspectives, *Bioact. Mater.*, 2024, **38**, 346–373, DOI: 10.1016/J.BIOACTMAT.2024.04.032.

45 M. Rea, L. Di Lisa, G. Pagnotta, N. Gallo, L. Salvatore, F. D'Amico, N. Campilio, J. M. Baena, J. A. Marchal, A. F. G. Cicero, C. Borghi and M. L. Focarete, Establishing a Bioink Assessment Protocol: GelMA and Collagen in the Bioprinting of a Potential In Vitro Intestinal Model, *ACS Biomater. Sci. Eng.*, 2025, **11**(4), 2456–2467, DOI: 10.1021/ACSBIOMATERIALS.5C00034/ASSET/IMAGES/LARGE/AB5C00034_0009.JPEG.

46 R. N. Ghosh, J. Thomas, B. R. Vaidehi, N. G. Devi, A. Janardanan, P. K. Namboothiri and M. Peter, An Insight into Synthesis, Properties and Applications of Gelatin Methacryloyl Hydrogel for 3D Bioprinting, *Mater. Adv.*, 2023, **4**(22), 5496–5529, DOI: 10.1039/D3MA00715D.

47 M. B. Łabowska, K. Cierluk, A. M. Jankowska, J. Kulbacka, J. Detyna and I. Michalak, A Review on the Adaption of Alginate-Gelatin Hydrogels for 3D Cultures and Bioprinting, *Materials*, 2021, **14**(4), 1–28, DOI: 10.3390/MA14040858.

48 A. Habib, V. Sathish, S. Mallik and B. Khoda, 3D Printability of Alginate-Carboxymethyl Cellulose Hydrogel, *Materials*, 2018, **11**, 454, DOI: 10.3390/MA11030454.

49 S. Morozkina, U. Strekalovskaya, A. Vanina, P. Snetkov, A. Krasichkov, V. Polyakova and M. Uspenskaya, The Fabrication of Alginate–Carboxymethyl Cellulose-Based Composites and Drug Release Profiles, *Polymers*, 2022, **14**(17), 3604, DOI: 10.3390/POLYM14173604.

50 A. A. Aldana, F. Valente, R. Dilley and B. Doyle, Development of 3D Bioprinted GelMA-Alginate Hydrogels with Tunable Mechanical Properties, *Bioprinting*, 2021, **21**, e00105, DOI: 10.1016/J.BPRINT.2020.E00105.

51 A. A. Abramov, M. K. Okisheva, P. Y. Tsygankov and N. V. Menshutina, Development of "Ink" for Extrusion Methods of 3D Printing with Viscous Materials, *Russ. J. Gen. Chem.*, 2023, **93**(12), 3264–3271, DOI: 10.1134/S1070363223120289/FIGURES/3.

52 N. Paxton, W. Smolan, T. Böck, L. Ouyang, R. Yao, Y. Zhao and W. Sun, Effect of Bioink Properties on Printability and Cell Viability for 3D Bioplotting of Embryonic Stem Cells, *Biofabrication*, 2016, **8**(3), 035020, DOI: 10.1088/1758-5090/8/3/035020.

53 V. H. M. Mouser, F. P. W. Melchels, J. Visser, W. J. A. Dhert, D. Gawlitta and J. Malda, Yield Stress Determines Bioprintability of Hydrogels Based on Gelatin-Methacryloyl and Gellan Gum for Cartilage Bioprinting, *Biofabrication*, 2016, **8**(3), 035003, DOI: 10.1088/1758-5090/8/3/035003.

54 C. Pellet and M. Cloitre, The Glass and Jamming Transitions of Soft Polyelectrolyte Microgel Suspensions, *Soft Matter*, 2016, **12**(16), 3710–3720, DOI: 10.1039/C5SM03001C.

55 R. A. Mohamed Yunus, M. Koch, P. Dieudonné-George, D. Truzzolillo, R. H. Colby and D. Parisi, Water-Driven Sol-Gel Transition in Native Cellulose/1-Ethyl-3-Methylimidazolium Acetate Solutions, *ACS Macro Lett.*, 2024, **20**, 219–226, DOI: 10.1021/ACSMACROLETT.3C00710/SUPPL_FILE/MZ3C00710_SI_003.MP4.

56 L. van Westerveld, J. Es Sayed, M. de Graaf, A. H. Hofman, M. Kamperman and D. Parisi, Hydrophobically Modified Complex Coacervates for Designing Aqueous Pressure-Sensitive Adhesives, *Soft Matter*, 2023, **19**(45), 8832–8848, DOI: 10.1039/D3SM01114C.

57 M. Khoonkari, J. Es Sayed, M. Oggioni, A. Amirsadeghi, P. Dijkstra, D. Parisi, F. Kruyt, P. van Rijn, M. K. Włodarczyk-Biegun and M. Kamperman, Bioinspired Processing: Complex Coacervates as Versatile Inks for 3D Bioprinting, *Adv. Mater.*, 2023, **35**(28), 2210769, DOI: 10.1002/ADMA.202210769.

58 C. Kaliampakou, N. Lagopati, E. A. Pavlatou and C. A. Charitidis, Alginate–Gelatin Hydrogel Scaffolds; An Optimization of Post-Printing Treatment for Enhanced Degradation and Swelling Behavior, *Gels*, 2023, **9**, 857, DOI: **10.3390/GELS9110857**.

59 D. B. Andrade, L. L. S. Soares, F. L. A. Cardoso, I. S. Lima, J. G. V. Silva, M. A. M. Carvalho, M. G. Fonseca, G. Brito, C. de, F. E. P. Santos, J. A. Osajima, A. O. Lobo and E. C. Silva-Filho, Hydrogel Based on Nanoclay and Gelatin Methacrylate Polymeric Matrix as a Potential Osteogenic Application, *J. Funct. Biomater.*, 2023, **14**(2), 74, DOI: **10.3390/JFB14020074**.

60 M. Bercea, Rheology as a Tool for Fine-Tuning the Properties of Printable Bioinspired Gels, *Molecules*, 2023, **28**, 2766, DOI: **10.3390/MOLECULES28062766**.

61 S. Han, C. M. Kim, S. Jin and T. Y. Kim, Study of the Process-Induced Cell Damage in Forced Extrusion Bioprinting, *Biofabrication*, 2021, **13**(3), 035013, DOI: **10.1088/1758-5090/AC0415**.

62 S. Tuladhar, S. Clark and A. Habib, Tuning Shear Thinning Factors of 3D Bio-Printable Hydrogels Using Short Fiber, *Materials*, 2023, **16**, 572, DOI: **10.3390/MA16020572**.

63 A. Blaeser, D. F. Duarte Campos, U. Puster, W. Richtering, M. M. Stevens and H. Fischer, Controlling Shear Stress in 3D Bioprinting Is a Key Factor to Balance Printing Resolution and Stem Cell Integrity, *Adv. Healthcare Mater.*, 2016, **5**(3), 326–333, DOI: **10.1002/ADHM.201500677**.

64 W. Lim, G. J. Kim, H. W. Kim, J. Lee, X. Zhang, M. G. Kang, J. W. Seo, J. M. Cha, H. J. Park, M. Y. Lee, S. R. Shin, S. Y. Shin and H. Bae, Kappa-Carrageenan-Based Dual Crosslinkable Bioink for Extrusion Type Bioprinting, *Polymers*, 2020, **12**, 2377, DOI: **10.3390/POLYM12102377**.

65 S. Sakai and T. Morita, One-Step FRESH Bioprinting of Low-Viscosity Silk Fibroin Inks, *ACS Biomater. Sci. Eng.*, 2022, **8**(6), 2589–2597, DOI: **10.1021/ACSBIOMATERIALS.2C00269/SUPPL_FILE/AB2C00269_SI_001.PDF**.

66 P. B. Sathish, S. Gayathri, J. Priyanka, S. Muthusamy, R. Narmadha, G. S. Krishnakumar and R. Selvakumar, Tricomposite Gelatin-Carboxymethylcellulose-Alginate Bioink for Direct and Indirect 3D Printing of Human Knee Meniscal Scaffold, *Int. J. Biol. Macromol.*, 2022, **195**, 179–189, DOI: **10.1016/J.IJBIOMAC.2021.11.184**.

67 R. I. R. Ibañez, R. J. F. C. Do Amaral, R. L. Reis, A. P. Marques, C. M. Murphy and F. J. O'brien, 3D-Printed Gelatin Methacrylate Scaffolds with Controlled Architecture and Stiffness Modulate the Fibroblast Phenotype towards Dermal Regeneration, *Polymers*, 2021, **13**, 2510, DOI: **10.3390/POLYM13152510**.

68 A. E. Chalard, A. W. Dixon, A. J. Taberner and J. Malmström, Visible-Light Stiffness Patterning of GelMA Hydrogels Towards In Vitro Scar Tissue Models, *Front. Cell Dev. Biol.*, 2022, **10**, 946754, DOI: **10.3389/FCELL.2022.946754/BIBTEX**.

69 J. Kim, C. M. Hope, N. Gantumur, G. B. Perkins, S. O. Stead, Z. Yue, X. Liu, A. U. Asua, F. D. Kette, D. Penko, C. J. Drogemuller, R. P. Carroll, S. C. Barry, G. G. Wallace and P. T. Coates, Encapsulation of Human Natural and Induced Regulatory T-Cells in IL-2 and CCL1 Supplemented Alginate-GelMA Hydrogel for 3D Bioprinting, *Adv. Funct. Mater.*, 2020, **30**(15), 2000544, DOI: **10.1002/ADFM.202000544**.

70 H. Li, Y. J. Tan, R. Kiran, S. B. Tor and K. Zhou, Submerged and Non-Submerged 3D Bioprinting Approaches for the Fabrication of Complex Structures with the Hydrogel Pair GelMA and Alginate/Methylcellulose, *Addit. Manuf.*, 2021, **37**, 101640, DOI: **10.1016/J.ADDMA.2020.101640**.

71 K. Dubbin, A. Tabet and S. C. Heilshorn, Quantitative Criteria to Benchmark New and Existing Bio-Inks for Cell Compatibility, *Biofabrication*, 2017, **9**(4), 044102, DOI: **10.1088/1758-5090/AA869F**.